

Variational quantum policies for reinforcement learning

Sofiene Jerbi,¹ Casper Gyurik,² Simon Marshall,² Hans J. Briegel,^{1,3} and Vedran Dunjko²

¹*Institute for Theoretical Physics, University of Innsbruck, Technikerstr. 21a, A-6020 Innsbruck, Austria*

²*Leiden University, Niels Bohrweg 1, 2333 CA Leiden, Netherlands*

³*Department of Philosophy, University of Konstanz, Fach 17, 78457 Konstanz, Germany*

(Dated: March 1, 2025)

Variational quantum circuits have recently gained popularity as quantum machine learning models. While considerable effort has been invested to train them in supervised and unsupervised learning settings, relatively little attention has been given to their potential use in reinforcement learning. In this work, we leverage the understanding of quantum policy gradient algorithms in a number of ways. First, we investigate how to construct and train reinforcement learning policies based on variational quantum circuits. We propose several designs for quantum policies, provide their learning algorithms, and test their performance on classical benchmarking environments. Second, we show the existence of task environments with a provable separation in performance between quantum learning agents and any polynomial-time classical learner, conditioned on the widely-believed classical hardness of the discrete logarithm problem. We also consider more natural settings, in which we show an empirical quantum advantage of our quantum policies over standard neural-network policies. Our results constitute a first step towards establishing a practical near-term quantum advantage in a reinforcement learning setting. Additionally, we believe that some of our design choices for variational quantum policies may also be beneficial to other models based on variational quantum circuits, such as quantum classifiers and quantum regression models.

I. INTRODUCTION

With the advent of the Noisy Intermediate-Scale Quantum (NISQ) era [1, 2], variational quantum algorithms [3] have received a great deal of attention in the quantum computing community. Given access to state-of-the-art devices of sizes ranging between 50 and 100 qubits, the aim of variational algorithms is to leverage their full potential to achieve a quantum advantage in practical applications, i.e., beyond the contrived problems for which quantum supremacy was first claimed [4, 5].

Among the various areas of application of variational quantum algorithms, machine learning (ML) stands out as an area of both great practicality and flexibility: the broad scope of both classical and quantum ML together with the potential robustness of ML algorithms to noise (at least in the data) give it the potential to become a “killer application” for near-term devices. With this perspective in mind, several designs of quantum models for ML have been proposed. The most studied family of such models is that of so-called *variational quantum circuits* (VQCs) [6], sometimes also referred to as *quantum neural networks* [7, 8] due to the similar roles and training mechanisms they share with deep neural networks (DNNs). Among other tasks, VQCs have been successfully trained to solve classification tasks [8–11], generative modeling [12, 13] and clustering problems [14], and some results have been hinting toward their potential practical quantum advantage [10, 15–17]. In more recent considerations, the fundamental question of expressivity and trainability of VQCs [18–22] has received an increased amount of attention. This area of research has become of critical importance, particularly in light of results that show the existence of barren plateaus in the optimization landscapes of VQCs [23, 24].

Despite being one of the three main paradigms of ML, reinforcement learning (RL) [25] has been explored by very few works [26–30], especially as a potential near-term area of application [31–34]. This may be explained by the apparent complexity of what constitutes state-of-the-art RL systems like AlphaGo [35], making it unclear how near-term quantum enhancements could substantially improve these systems. Nevertheless, at the core of cutting-edge RL machinery are methods that are very similar to those used in supervised and unsupervised learning, and that could hence benefit from similar quantum enhancements. A notable component prone to quantum generalizations are the parametrized policies used in modern RL methods such as policy gradient [36] and actor-critic RL [37]. Due to their success in other areas of ML, DNNs specifying probability distributions over actions given states quickly became the standard policies used in deep RL. VQCs appear then as natural candidates for their quantum generalization.

In this work, we explore the trainability of quantum policies based on VQCs in classical RL environments. We discuss different choices of models, for which we set up the required mathematical formalisms, describe associated learning mechanisms, and show numerically the influence of several design choices on learning performance. For our numerical investigation, we first consider classical benchmarking environments, for which good and simple DNN policies are known, and in which we demonstrate that VQC policies can achieve a comparable performance. Inspired by the classification task of Havlíček *et al.* [10], which the authors conjecture to be classically hard, we also construct RL task environments where we show an empirical advantage of our VQC policies over the standard DNN policies used in deep RL. Following this direction, we construct RL environments with a provable

gap in performance between a family of VQC policies and any classical learner. These environments essentially build up on the work of Liu *et al.* [16] by embedding the discrete logarithm problem (DLP) into a learning setting, which naturally makes one consider VQC policies based on Shor’s algorithm [38] to solve them.

The recent results of Schuld *et al.* [18] suggest that training VQC classifiers on “nicely-behaving” labeling functions is not easy, since these naturally represent periodic and (highly-)oscillating functions. Training models for RL is known to be even harder than classifiers, due to the additional temporal structure of RL tasks and the need for policy families that allow for both exploratory and exploitative behavior. This added difficulty makes it unclear whether VQCs constitute well-suited policy families for RL. We show nonetheless that VQCs can be trained to good performance in benchmarking environments. However, we find this performance to be very much model-dependent, and the learned policies to be quite complex compared to DNN policies. We posit that the difficulty of training VQC policies on these benchmarking tasks comes from a mismatch with the natural policies represented by VQCs. To support this hypothesis, we show numerically the existence of proof-of-concept environments where VQC policies have a greater learning performance than standard DNNs. We further strengthen our claims by constructing RL environments with a provable quantum advantage of a class of VQC policies over any efficient classical learner, conditioned on the widely-believed classical hardness of DLP.

Our results constitute, to our knowledge, the best-achieved performance of quantum policies in classical RL tasks and provide the first numerical evidence of a separation between quantum and classical policies in RL.

We present our results as follows: Sec. III introduces the fundamental concepts behind policy gradient methods in RL. Sec. IV gives a detailed construction of our VQC policies and their learning algorithms. Sec. V presents our numerical investigation of the performance of these policies in benchmarking environments. Sec. VI A describes the construction of RL environments with a provable separation between a class of quantum agents and any efficient classical learner. Sec. VI B describes RL environments for which we show an empirical quantum advantage of our VQC policies over DNN policies.

II. RELATED WORK

Recently, a few works have been exploring variational approaches for RL. Among these, Refs. [31, 32] trained VQC-based agents in classical RL environments. However, these take a value-based approach to RL, meaning that they use VQCs as value-function approximators instead of direct policies (see Sec. III A for a clarification of this distinction). Their agents achieve a lower performance in benchmarking environments (namely, the Cart-Pole environment), which we believe can be improved

using some of our considerations on training VQCs for RL (i.e., trainable observables and input scaling parameters). An actor-critic approach to QRL was introduced in Ref. [33], where the agents train both a VQC actor (or policy) and a VQC critic (or value-function approximator). In contrast to our work, these are trained in quantum environments (e.g., quantum-control environments), that provide a quantum state to the agent, and the latter acts back with a continuous classical action. Finally, Ref. [34] describes a variational algorithm for value-based RL. The function-approximation models on which this algorithm is applied are energy-based models (e.g., deep and quantum Boltzmann machines), hence not VQCs.

III. TRAINING POLICIES FOR RL

In this section, we introduce the fundamental concepts and methods behind the policy gradient approach in RL. These notions will give us all the tools to develop our variational quantum policies and their learning algorithms in the next section. A general description of the framework we work in is given in Fig. 1.

A. Value-function optimization

At the core of policy gradient methods are two ingredients: a parametrized policy π_{θ} , that governs an agent’s actions in an environment, and its associated value function $V_{\pi_{\theta}}$, which evaluates the long-term performance of this policy in the environment. The policy π_{θ} belongs to a family Π_{θ} of conditional probability distributions over actions given states, where each element of this family is parametrized by a vector of parameters $\theta \in \mathbb{R}^d$. When acting with a fixed policy in a fixed environment, an agent collects a sequence of rewards that depends both on its policy and the environment (probabilistic) dynamics. Since the goal of RL problems is not to simply maximize immediate rewards at each interaction step but additionally *long-term* rewards, a figure of merit assessing the performance of an agent should hence measure the accumulation of “all” of its expected rewards. This figure of merit is called the value function of a policy π_{θ} and a common formulation is given by the expected return:

$$V_{\pi_{\theta}}(s) = \mathbb{E}_{\pi_{\theta}, P_E} \left[\sum_{t=0}^{H-1} \gamma^t r_t \right] = \mathbb{E}_{\pi_{\theta}, P_E} [R(\tau)] \quad (1)$$

where s is the initial state of the agent’s interaction τ with the environment, P_E a description of the environment dynamics (e.g., in the form of an MDP), and r_t the collected reward at timestep t of this interaction. Each interaction has a horizon (or length) $H \in \mathbb{N} \cup \{\infty\}$ and the expected returns typically involve a discount factor $\gamma \in [0, 1]$ that allows, when $\gamma < 1$, to avoid diverging value functions for a horizon $H = \infty$.

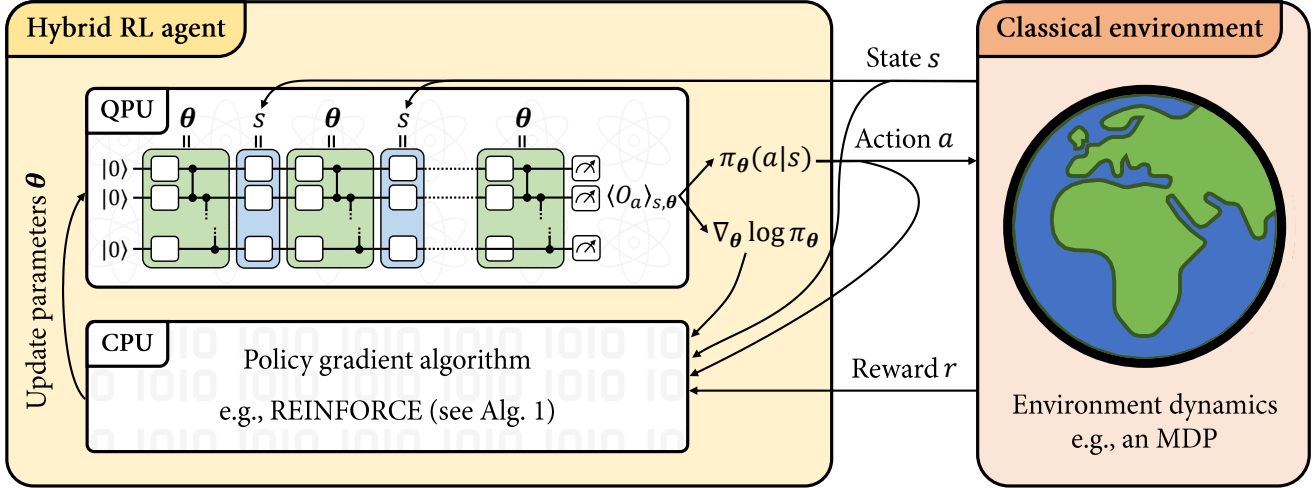


Figure 1. **Training variational quantum policies for reinforcement learning.** We consider a quantum-enhanced RL scenario where a hybrid quantum-classical agent learns by interacting with a classical environment. This interaction is split into episodes, each consisting of a cyclic sequence of states, actions and rewards. For each state s it perceives, the agent deliberates on its next action a according to its policy $\pi_\theta(a|s)$ and perceives feedback on its behavior in the form of a reward r . For our hybrid agents, the policy π_θ is specified by a VQC (see Defs. 1 and 2) evaluated (along with the gradient $\nabla_\theta \log \pi_\theta$) on a quantum processing unit (QPU). The training of this policy is performed by a classical learning algorithm (running on a classical processing unit (CPU)), such as the REINFORCE algorithm (see Alg. 1), which uses sample episodes and policy gradients to update the policy parameters θ . The environment dynamics are described by, e.g., a Markov decision process (MDP) [25].

Policy gradient methods take a direct optimization approach to RL: starting from an initial policy $\pi_\theta \in \Pi_\theta$, its parameters are iteratively updated such as to maximize its associated value function $V_{\pi_\theta}(s)$, typically via gradient ascent.¹ For this method to be applicable, one should be able to evaluate the value function of the trained policy, or at least its gradient $\nabla_\theta V_{\pi_\theta}$. As we explain in the next subsection, these two quantities can be estimated by collecting episodes of interaction for policies $\pi_{\theta'}$, where θ' is either exactly the agent's θ or close to it in ℓ_∞ norm.

B. Policy gradient theorem

The most straightforward approach to estimate the value function of a policy is via a Monte Carlo approach: by collecting N episodes τ of interaction governed by π_θ , one can compute for each of these the discounted return $R(\tau)$ appearing in Eq. (1) and average the results. The resulting value

$$\tilde{V}_{\pi_\theta}(s) = \frac{1}{N} \sum_{i=1}^N \sum_{t=0}^{H-1} \gamma^t r_{i,t} \quad (2)$$

¹ This fundamentally differs from value-based methods in RL, that start by defining an approximate value function \tilde{V}_ω (now taking as input a state *and* an action) and iteratively update ω such as to fit the value function of a policy that is directly derived from \tilde{V}_ω , e.g., $\pi(a|s) = \text{softmax}_a(\tilde{V}_\omega(s, a))$.

is a so-called Monte Carlo estimate of the value function. With the capacity to estimate the value function, we can also estimate its gradient using, e.g., numerical means: by evaluating $\tilde{V}_{\pi_\theta}(s)$ and $\tilde{V}_{\pi_{\theta+\delta\theta}}(s)$ for various “1-hot” vectors $\delta\theta = (0, \dots, 0, 1, 0, \dots, 0)$, we can use finite-difference methods to return an estimate of $\nabla_\theta V_{\pi_\theta}(s)$. This approach, despite being simple and compatible with non-differentiable policies, has a sample complexity (in terms of number of episodes N to be collected) that scales linearly in the dimension of θ . Perhaps the most appealing aspect of policy gradient methods is that the gradients of value functions also have an analytical formulation whose evaluation has a sample complexity only logarithmic in the dimension of θ [39]. This analytical formulation is known as the policy gradient theorem and is restated below for completeness:

Theorem 1 (Policy gradient theorem (PGT) [36]). *Given an environment defined by its dynamics P_E , the gradient of a value function V_{π_θ} , as defined by Eq. (1), with respect to the parameters θ of its associated policy π_θ , is given by*

$$\begin{aligned} \nabla_\theta V_{\pi_\theta}(s) &= \mathbb{E}_{\pi_\theta, P_E} \left[\sum_{t=0}^{H-1} \nabla_\theta \log \pi_\theta(a_t|s_t) V_{\pi_\theta}(s_t) \right] \quad (3) \\ &= \mathbb{E}_{\pi_\theta, P_E} \left[\sum_{t=0}^{H-1} \frac{\nabla_\theta \pi_\theta(a_t|s_t)}{\pi_\theta(a_t|s_t)} V_{\pi_\theta}(s_t) \right] \end{aligned}$$

Essentially, due to the so-called “log-likelihood trick” [40], the differentiation with respect to the policy param-

Algorithm 1: REINFORCE with VQC policies and value-function baselines

Input: a VQC policy π_θ from Defs. 1 or 2
Input: a differentiable value-function approximator \tilde{V}_ω

1 Initialize parameters θ and ω ;
2 **while** *True* **do**
3 Generate N episodes $\{(s_0, a_0, r_1, \dots, s_{H-1}, a_{H-1}, r_H)\}_i$ following π_θ ;
4 **for** *episode i* **in batch do**
5 Compute the returns $G_{i,t} \leftarrow \sum_{t'=1}^{H-t} \gamma^{t'} r_{t+t'}$;
6 Compute the gradients $\nabla_\theta \log \pi_\theta(a_t^{(i)} | s_t^{(i)})$ using Lemma 1;
7 Fit $\{\tilde{V}_\omega(s_t^{(i)})\}_{i,t}$ to the returns $\{G_{i,t}\}_{i,t}$;
8 Compute

$$\Delta\theta = \frac{1}{N} \sum_{i=1}^N \sum_{t=0}^{H-1} \nabla_\theta \log \pi_\theta(a_t^{(i)} | s_t^{(i)}) (G_{i,t} - \tilde{V}_\omega(s_t^{(i)}))$$
;
9 Update $\theta \leftarrow \theta + \alpha \Delta\theta$;

eters can be made to act solely on the random variables “inside” the expected value, while leaving the probability distribution behind this expected value unchanged. This means that the gradient of the value function can, similarly to the value function itself, be estimated via Monte Carlo rollouts in the environment (now only governed by a fixed π_θ) and environment-independent computations (i.e., the evaluation of $\nabla_\theta \log \pi_\theta(a_t | s_t)$).

C. Baselines

In practice, the value-function terms $V_{\pi_\theta}(s_t)$ appearing in Eq. (3) are estimated in one of two main ways: either from the rewards collected during Monte Carlo rollouts in the environment (i.e., using \tilde{V}_{π_θ} from Eq. (2)), which leads to a learning algorithm called REINFORCE [25, 41]; or via the use of an additional value-function approximator \tilde{V}_ω (e.g., a DNN), turning this approach into a so-called actor-critic method (the actor being the policy and the critic the value-function approximator) [37, 42]. To study the simplest scenario without the influence of a critic on the learning performance, we consider a REINFORCE implementation in the remainder of this paper.

A known limitation of the REINFORCE algorithm however is that Monte Carlo estimates \tilde{V}_{π_θ} have in general a very high variance [43], which can severely limit the performance of the agents in certain environments (e.g., the MountainCar environment we consider in Sec. V). A simple variance-reduction technique goes through the use of a so-called *baseline* $b(s_t)$, which is a real-valued function used as follows in the policy gradient theorem:

$$\nabla_\theta V_{\pi_\theta}(s) = \mathbb{E} \left[\sum_{t=0}^{H-1} \nabla_\theta \log \pi_\theta(a_t | s_t) (V_{\pi_\theta}(s_t) - b(s_t)) \right]$$

It can easily be shown that the addition of this baseline does not bias the expected value above [44], and that an approximation of the value function \tilde{V}_ω is in a general a good choice of baseline [43]². For some of the benchmarking environments in Sec. V, we hence rely on simple value-function baselines, identical to those commonly used to evaluate the performance of REINFORCE in these environments [45].

IV. THE RAW-VQC AND SOFTMAX-VQC POLICIES

Having introduced the underlying notions behind policy gradient methods, we now construct policy families based on VQCs and describe their training algorithm. We consider two main families of VQC policies. The first, which we refer to as the raw-VQC model, is motivated by quantum classifiers in supervised learning tasks, and uses the natural Born rule of quantum measurements to derive a policy from a VQC. Additionally, we define a new model which differs from the first by its adjustable greediness, i.e., the natural Born-type distribution of a VQC can be made more or less peaked through an additional degree of control. We achieve this additional property by using a softmax function (or Gibbs distribution) to transform the output of quantum circuits, leading to our softmax-VQC model. This consideration arises naturally in a reinforcement learning context where an agent’s policy needs to shift from an exploratory behavior (i.e., close to uniform distribution) to a more exploitative behavior (i.e., a peaked distribution). It is however absent in a supervised learning (SL) setting, where quantum classifiers are naturally made deterministic by using an argmax function (i.e., a very strong softmax) to assign labels to datapoints.

A. Models definition

At the core of our variational quantum policies is a VQC defined by a unitary $U(s, \theta)$ acting on n qubits. This unitary encodes an input state $s \in \mathbb{R}^d$ and is parametrized by a trainable vector θ . Throughout our numerical experiments (Sec. V and VIB), we only consider VQCs from the hardware-efficient family [46], with an alternating-layered architecture [18, 47]. This architecture is depicted in Fig. 2 and essentially consists in an alternation of D_{enc} encoding layers (composed of single-qubit rotations) and $D_{\text{enc}} + 1$ variational layers (composed of single-qubit rotations and entangling gates). Note however that the quantum policies we define below are compatible with more general VQC architectures.

² Note that the REINFORCE algorithm with a value-function baseline is different from actor-critic methods, as the former still relies on Monte Carlo estimates \tilde{V}_{π_θ} to compute the gradient $\nabla_\theta V_{\pi_\theta}$.

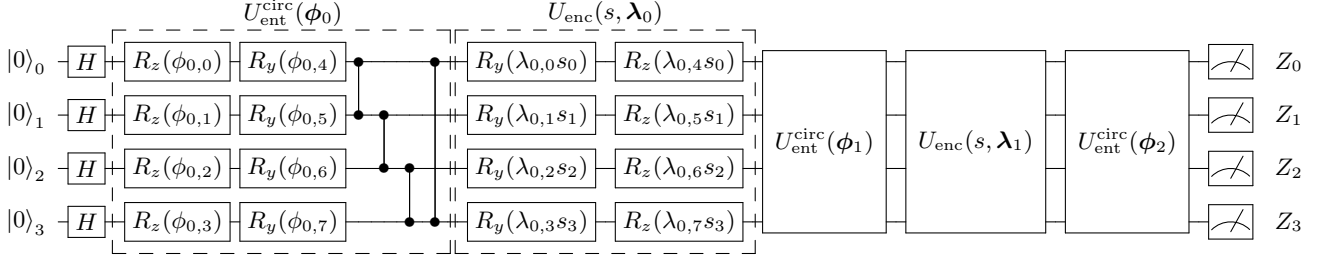


Figure 2. VQC architecture for $n = 4$ qubits, depth $D_{\text{enc}} = 2$, and a circular topology of entangling layers. This architecture is composed of alternating layers of encoding unitaries $U_{\text{enc}}(s, \lambda_i)$ taking as input a state vector $s = (s_0, \dots, s_{d-1})$ and scaling parameters λ_i (part of a vector $\lambda \in \mathbb{R}^{|\lambda|}$ of dimension $|\lambda|$), and entangling unitaries $U_{\text{ent}}(\phi_i)$ taking as input rotation angles ϕ_i (part of a vector $\phi \in [0, 2\pi]^{|\phi|}$ of dimension $|\phi|$). These are built out of single-qubit Pauli rotations R_z and R_y , and entangling gates such as CZ gates. We also consider architectures with trainable entangling gates (Pauli R_{zz} rotations) and/or an all-to-all entangling connectivity (as opposed to circular here). The VQC is measured in a given basis (here the computational basis), so as to sample an eigenvalue of an observable O_a , and estimate its expectation value $\langle O_a \rangle_{s, \theta}$ through repeated evaluations.

When applied on a certain input state (wlog., $|0^{\otimes n}\rangle$), the VQC unitary $U(s, \theta)$ produces a quantum state $|\psi\rangle \in \mathcal{H} \subset \mathbb{C}^{2^n}$. If measured in the computational basis, the quantum state $|\psi\rangle$ naturally collapses to a basis state of \mathcal{H} whose probability distribution follows the Born rule. It is hence intuitive to consider using this distribution as the policy of an RL agent. For that, all we need to do is partition all computational basis states of \mathcal{H} in $|A|$ disjoint subspaces, where $|A|$ is the number of actions available to the agent³. This definition allows very efficient sampling from the agent’s policy, as only one preparation of $|\psi\rangle$ is required to generate a sample from $\pi_\theta(a|s)$. We will see however in the next subsection that one sample/preparation is not enough to train this policy using the policy gradient theorem (it requires the estimation of expectation values). But first, we give a more formal definition of **raw-VQC** policies.

Definition 1 (raw-VQC). *Given a VQC acting on n qubits, taking as input a state $s \in \mathbb{R}^d$, rotation angles $\phi \in [0, 2\pi]^{|\phi|}$ and scaling parameters $\lambda \in \mathbb{R}^{|\lambda|}$, such that its corresponding unitary $U(s, \phi, \lambda)$ produces the quantum state $|\psi_{s, \phi, \lambda}\rangle = U(s, \phi, \lambda)|0^{\otimes n}\rangle$, we define its associated raw-VQC policy as:*

$$\pi_\theta(a|s) = \langle P_a \rangle_{s, \theta} \quad (4)$$

where $\langle P_a \rangle_{s, \theta} = \langle \psi_{s, \phi, \lambda} | P_a | \psi_{s, \phi, \lambda} \rangle$ is the expectation value of a projector P_a associated to action a , such that $\sum_a P_a = I$ and $P_a P_{a'} = \delta_{a, a'}$. $\theta = (\phi, \lambda)$ constitute all the trainable parameters of this policy.

In the definition of our VQCs, we include trainable *scaling parameters* λ . As their name suggests, these are used in every encoding gate of our VQC to re-scale its input components (i.e., state components, in the case of quantum policies). This modification to the standard

data encoding in quantum classifiers is justified by recent considerations on the structure of VQC functions. As pointed out by Schuld *et al.* [48], for general Hermitian observables O_a and a general input encoding using rotation angles of gates of the form e^{isH} (H an arbitrary Hamiltonian, e.g., a Pauli matrix), expectation values $\langle O_a \rangle_{s, \theta}$, taken as a function of s , can be expressed as Fourier series of finite degree K . Moreover, in the special case where single-qubit Pauli rotations $e^{i\sigma s_j/2}$ are used to encode a given component, the spectrum of this Fourier series is entirely integer-valued and its degree K is upper-bounded by the number of repetitions of the Pauli-rotation encodings (in our case, $K \leq 2D_{\text{enc}}$). This result leads to two main constraints on the accessible VQC functions/policies without scaling parameters: these are periodic functions of the input components s_j with period at most 2π , and the depth D_{enc} is limiting the size and range of their frequency spectrum. Hence, very special care should be dedicated to the choice of depth of the VQC (in number of alternating layers) and to the range of its input components. To work around these limitations, we choose to include the *scaling parameters* λ , that are trained along with the other VQC parameters. These trainable parameters allow access to a wider and richer spectrum of frequencies, and hence provide shallow VQCs with more expressive power. We detail in Sec. IV B how to train these parameters.

The main limitation of raw-VQC policies is that their greediness can not be directly adjusted. The only means for a raw-VQC policy to become more greedy is for its rotation angles ϕ to shift amplitudes of the quantum state $|\psi_{s, \phi, \lambda}\rangle$ to the subspace associated to the action $\text{argmax}_a \langle P_a \rangle_{s, \theta}$. Moreover, this transformation of the rotation angles ϕ would need to act close to independently from the input state s for it to only adjust the greediness of the policy (and not the most likely actions). This makes the task of switching between an exploratory and an exploitative policy relatively challenging for a raw-VQC. A solution to this problem, that

³ Note that this is only possible if \mathcal{H} is a Hilbert space of dimension $2^n \geq |A|$.

preserves the differentiability of the VQC policy, is to apply a non-linear activation function such as a softmax on the probabilities $\langle P_a \rangle_{s, \theta}$. The resulting softmax-VQC model has now an inverse-temperature parameter β that can be used to adjust the greediness of its associated policy, e.g., through an annealing schedule on β . Furthermore, by noting that the input of a softmax function does not need to be normalized nor strictly positive for it to return a valid probability distribution, we can replace the projectors P_a by general Hermitian operators⁴ O_a . We generalize these observables one step further and take them to be weighted combinations of some (action-specific) Hermitian operators $H_{a,i}$, with trainable weights $w_{a,i}$. These weights allow our agents to have a direct degree of control over the greediness of their policy. A formal definition of softmax-VQC policies is given below.

Definition 2 (softmax-VQC). *Given a VQC acting on n qubits, taking as input a state $s \in \mathbb{R}^d$, rotation angles $\phi \in [0, 2\pi]^{|\phi|}$ and scaling parameters $\lambda \in \mathbb{R}^{|\lambda|}$, such that its corresponding unitary $U(s, \phi, \lambda)$ produces the quantum state $|\psi_{s, \phi, \lambda}\rangle = U(s, \phi, \lambda)|0^{\otimes n}\rangle$, we define its associated softmax-VQC policy as:*

$$\pi_{\theta}(a|s) = \frac{e^{\beta \langle O_a \rangle_{s, \theta}}}{\sum_{a'} e^{\beta \langle O_{a'} \rangle_{s, \theta}}} \quad (5)$$

where $\langle O_a \rangle_{s, \theta} = \langle \psi_{s, \phi, \lambda} | \sum_i w_{a,i} H_{a,i} | \psi_{s, \phi, \lambda} \rangle$ is the expectation value of the weighted Hermitian operators $H_{a,i}$ associated to action a , and $\beta \in \mathbb{R}$ is an inverse-temperature parameter. $\theta = (\phi, \lambda, w)$ constitute all the trainable parameters of this policy.

B. Gradient expression

A prerequisite to train policies using the policy gradient theorem (see Thm. 1) is for their log-probability functions (or at least their probability functions) to be differentiable with respect to their parameters θ . We know that expectation values $\langle O_a \rangle_{s, \theta}$ of general Hermitian observables O_a measured on VQCs can be efficiently estimated up to additive error on quantum computers. We also know that these expectation values are differentiable w.r.t. θ , and that the evaluation of their gradient $\nabla_{\theta} \langle O_a \rangle_{s, \theta}$ up to additive error is only linear in the complexity of evaluating $\langle O_a \rangle_{s, \theta}$. This last point is due to two main formulations of the gradient $\nabla_{\theta} \langle O_a \rangle_{s, \theta}$: the finite-difference formulation

$$\partial_i \langle O_a \rangle_{s, \theta} \approx \frac{\langle O_a \rangle_{s, \theta + \varepsilon e_i} - \langle O_a \rangle_{s, \theta}}{\varepsilon}, \quad (6)$$

⁴ Note that lifting this restriction makes the implementation of our VQC policies on quantum devices not only compatible with projective measurements but also more general POVM (Positive Operator-Valued Measure) measurements.

and the analytic formulation (known as the parameter-shift rule [48, 49])⁵

$$\partial_i \langle O_a \rangle_{s, \theta} = \frac{\langle O_a \rangle_{s, \theta + \frac{\pi}{2} e_i} - \langle O_a \rangle_{s, \theta - \frac{\pi}{2} e_i}}{2}, \quad (7)$$

which both only require two evaluations of expectation values $\langle O_a \rangle_{s, \theta'}$.

These remarks show that it is straightforward to estimate $\nabla_{\theta} \log \pi_{\theta}(a|s)$ for raw-VQCs, since the probabilities $\pi_{\theta}(a|s)$ are direct expectation values of projectors measured on VQCs. However, in the case of softmax-VQCs, one can not intuitively tell whether this gradient can be expressed in terms of gradients of expectations values. Nonetheless, softmax probability functions are known to have a very interesting formulation of their log-gradient in terms of the gradient of their density function. This formulation naturally applies to softmax-VQCs as well, and we provide it in the next lemma (see Appendix A for a derivation).

Lemma 1. *Given a softmax-VQC policy π_{θ} , the gradient of its logarithm is given by:*

$$\nabla_{\theta} \log \pi_{\theta}(a|s) = \beta \left(\nabla_{\theta} \langle O_a \rangle_{s, \theta} - \sum_{a'} \pi_{\theta}(a'|s) \nabla_{\theta} \langle O_{a'} \rangle_{s, \theta} \right)$$

where the partial derivatives with respect to rotation angles $\partial_{\phi_i} \langle O_a \rangle_{s, \theta}$ and scaling parameters $\partial_{\lambda_i} \langle O_a \rangle_{s, \theta}$ can be estimated via a finite-difference method (Eq. (6)) or the parameter-shift rule (Eq. (7)); while partial derivatives with respect to observable weights are trivially given by $\partial_{w_{a,i}} \langle O_a \rangle_{s, \theta} = \langle \psi_{s, \phi, \lambda} | H_{a,i} | \psi_{s, \phi, \lambda} \rangle$ (see Def. 2).

For a raw-VQC policy π_{θ} , we have instead:

$$\nabla_{\theta} \log \pi_{\theta}(a|s) = \frac{\nabla_{\theta} \langle P_a \rangle_{s, \theta}}{\langle P_a \rangle_{s, \theta}} \quad (8)$$

where the partial derivatives $\partial_{\phi_i} \langle P_a \rangle_{s, \theta}$ and $\partial_{\lambda_i} \langle P_a \rangle_{s, \theta}$ can be estimated similarly to above.

Coming back on a remark made in Sec. IV A, we can clearly see from Eq. (8) that, while sampling from a raw-VQC policy requires only one evaluation of the VQC, training this policy with the PGT actually requires estimating the probabilities $\langle P_a \rangle_{s, \theta}$.

Note that the parameters λ do not act as direct rotation angles in the VQC, but are additionally multiplied by state components. This remark leads to the following expression for the derivatives w.r.t. $\lambda_{i,j}$ (see Fig. 2):

$$\partial_{\lambda_{i,j}} \langle O_a \rangle_{s, \theta} = s_j \frac{f_{i,j}(s_j \lambda_{i,j} + \frac{\pi}{2}) - f_{i,j}(s_j \lambda_{i,j} - \frac{\pi}{2})}{2}$$

where $f_{i,j}(\cdot)$ is a short-hand notation for $\langle O_a \rangle_{s, \theta}$ as a function of the rotation angle assigned to $s_j \lambda_{i,j}$.

⁵ This formulation of the parameter-shift rule applies to angles θ parametrizing gates of the form $e^{i\theta H}$ where H is a tensor product of Pauli operators. For more general unitary gates, see Ref. [48].

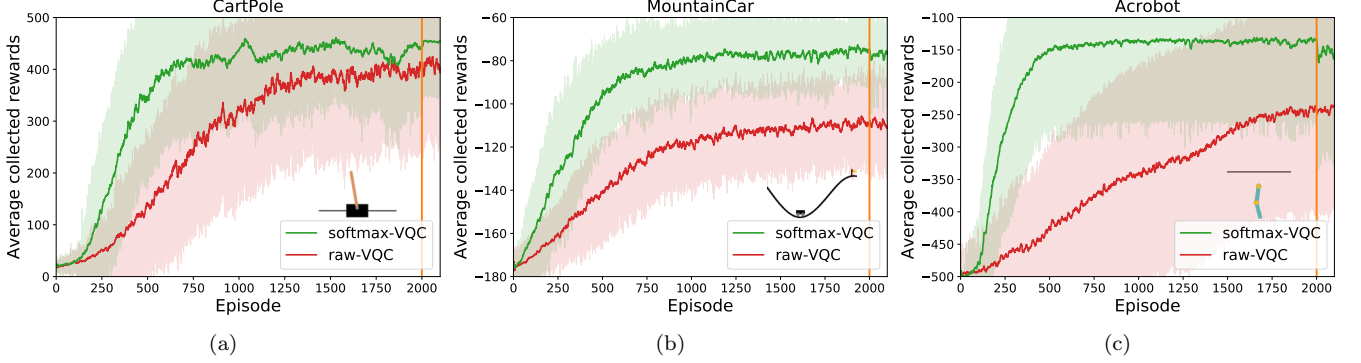


Figure 3. **Numerical evidence of the advantage of softmax-VQC over raw-VQC in benchmarking environments.** The learning curves (20 agents per curve) of randomly-initialized softmax-VQC agents (green curves) and raw-VQC agents (red curves) in OpenAI Gym environments: (a) CartPole-v1, (b) MountainCar-v0, and (c) Acrobot-v1. Each curve is temporally averaged with a time window of 10 episodes. All agents have been trained using the REINFORCE algorithm (see Alg. 1), with value-function baselines for the MountainCar and Acrobot environments. At episode 2000, the training of the agents is stopped and their performance is tested over 100 episodes, with a $\beta = 100$ for softmax-VQC agents. The delimitation between training and testing phases is represented by an orange vertical line.

C. Approximate policy sampling

A natural consideration when it comes to the implementation of softmax-VQCs is whether one can efficiently (in the number of evaluations of the VQC) sample from policies of the form of Eq. (5). In other terms, if one evaluates estimates $\widetilde{\langle O_a \rangle}_{s, \theta}$ of the expectation values $\langle O_a \rangle_{s, \theta}$ on a quantum computer, what precision is required in order for the resulting approximate policy $\widetilde{\pi}_\theta$ to produce samples close to those of the true π_θ ? We find that additive-error approximations of $\langle O_a \rangle_{s, \theta}$ lead to a policy that is close in total variation distance from the true π_θ . We state our result formally in the following lemma.

Lemma 2. *For a softmax-VQC policy π_θ defined by a unitary $U(s, \phi, \lambda)$ and observables $O_a = \sum_i w_{a,i} H_{a,i}$, call $\widetilde{\langle O_a \rangle}_{s, \theta}$ ε -close approximations (in additive error) of the expectation values of these observables with respect to $|\psi_{s, \phi, \lambda}\rangle$. Then the approximate policy*

$$\widetilde{\pi}_\theta(a|s) = \frac{e^{\beta \widetilde{\langle O_a \rangle}_{s, \theta}}}{\sum_{a'} e^{\beta \widetilde{\langle O_{a'} \rangle}_{s, \theta}}} \quad (9)$$

has total variation distance $\mathcal{O}(\varepsilon)$ to π_θ . Since expectation values can be efficiently estimated to additive error on a quantum computer, this implies efficient approximate sampling from π_θ .

The proof of this lemma is deferred to Appendix B.

We also obtain a similar result for the log-policy gradient of softmax-VQCs (see Lemma 1), that we show can be efficiently estimated to additive error in ℓ_∞ -norm (see Appendix C for a proof).

V. PERFORMANCE COMPARISON IN BENCHMARKING ENVIRONMENTS

In the previous section, we have introduced our quantum policies and described several of our design choices. Notably, we defined the raw-VQC and softmax-VQC models and introduced two original features for VQCs: trainable observables at their output and trainable scaling parameters for their input. Despite having provided theoretical justification for these choices, it is natural to evaluate their actual influence on learning performance. In the following section, we undertake this task through numerical simulations. More specifically, we consider standard classical benchmarking environments from the OpenAI Gym library [50] on which we compare the performance of our quantum policies.

A. CartPole, MountainCar and Acrobot

The task environments we consider in this section are three standard control tasks, commonly used to evaluate the performance of (simple) RL algorithms. All three have the specificity that their state space is continuous (of dimension d between 2 and 6), but that their action space is discrete and small (2 or 3 actions). Moreover, simple NN-policies, as well as simple closed-form policies, are known to perform very well in these environments [51], which makes them an excellent testbed to benchmark VQC policies. We defer the specifications of these environments to Appendix D.

B. raw-VQC v.s. softmax-VQC

In our first set of experiments, presented in Fig. 3, we evaluate the general performance of our proposed

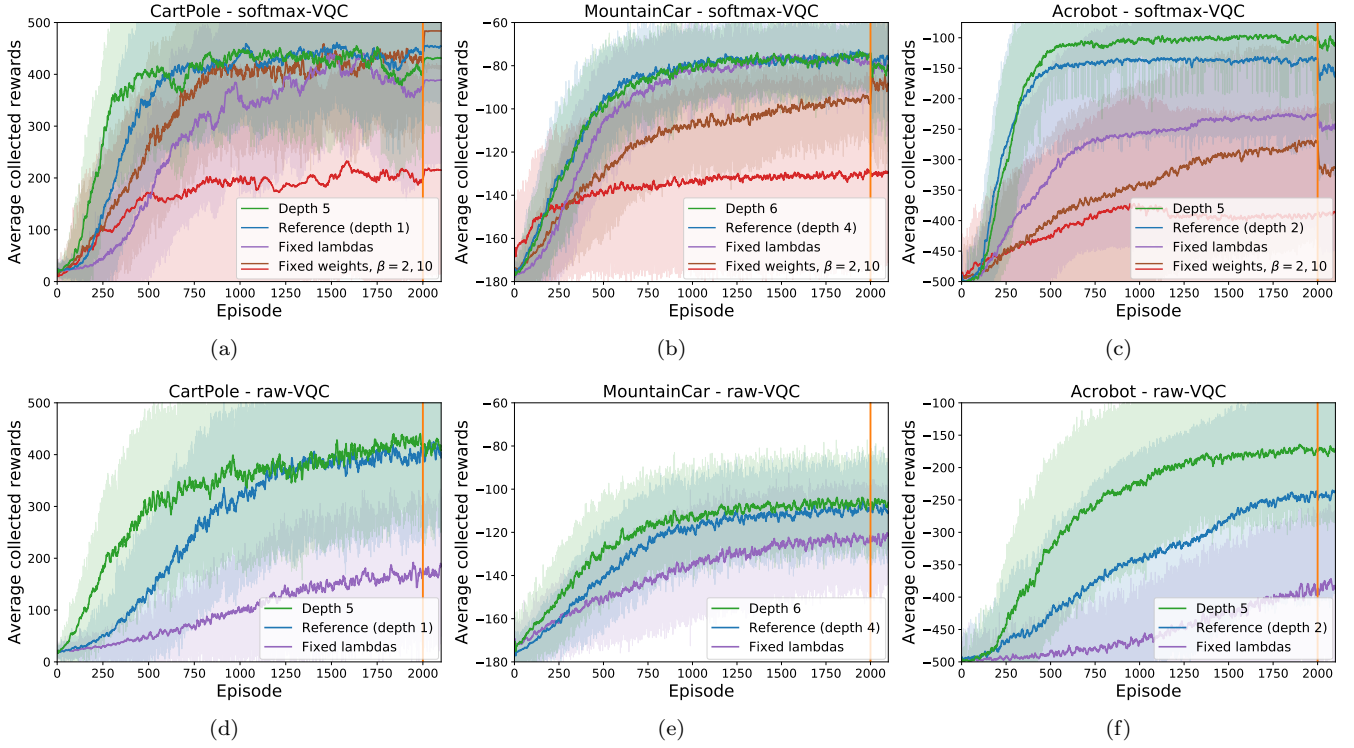


Figure 4. **Influence of the model architecture for softmax-VQC and raw-VQC agents.** (a) to (f) The blue curves in each plot correspond to the learning curves from Fig. 3. Other curves highlight the influence of individual hyperparameters, compared to the reference hyperparameters of the blue curves. Plots (a) to (c) focus on the softmax-VQC model, while plots (d) to (f) focus on the raw-VQC model. Each curve represents the average performance of 20 agents and is temporally averaged with a time window of 10 episodes. At episode 2000, the training of the agents is stopped and their performance is tested over 100 episodes, with a $\beta = 100$ for softmax-VQC agents. The delimitation between training and testing phases is represented by an orange vertical line.

quantum policies on classical environments. The aim of these experiments is twofold: first, showcase that quantum policies based on low-depth VQCs can be trained to good performance in benchmarking environments; second, we want to test the advantage of softmax-VQC policies over raw-VQC policies that we conjectured in the Sec. IV A. To assess these claims, we take a similar approach for each of our benchmarking environments, in which we evaluate the average learning performance of 20 raw-VQC and 20 softmax-VQC agents. The hyperparameters of these agents were selected in the following manner: apart from the VQC depth, the hyperparameters that these two models have in common were jointly picked (out of a hyperparameter search) such as to give the best overall performance for both groups of agents; the hyperparameters specific to each model were optimized independently. As for the VQC depth D_{enc} , the latter was chosen as the minimum depth for which near-optimal performance was observed for either raw-VQC or softmax-VQC agents (near-optimal with respect to the best performance observed for each models). The resulting learning curves confirm both our hypotheses: quantum policies can achieve good performance on the three benchmarking tasks that we consider, and we can see

a clear separation between the performance of softmax-VQC and raw-VQC agents, at least at low VQC-depth.

C. Influence of architectural choices

The results of the previous subsection however do not indicate if the separation we observe is still valid for deeper VQCs nor whether other design choices we have made in Sec. IV A had an influence on the performance of our quantum agents. To address these concerns, we run a second set of experiments, presented in Fig. 4. In these simulations, we again evaluate the average performance of our quantum agents but after modifying one of three design choices: we either increment the depth of the VQC (until no significant increase in performance is observed), fix the input-scaling parameters λ to **1**, or fix the observable weights \mathbf{w} of softmax-VQC agents to **1**. By comparing the performance of these agents with that of the agents from Fig. 3, we can make the following observations:

a. Influence of depth: increasing the depth of the VQC generally increases (not strictly) the performance of the quantum agents, more significantly for raw-VQC

agents. Nonetheless, we observe that, even at greater depth, the final performance as well as the speed of convergence of softmax-VQC agents remain greater than that of raw-VQC agents. Note that the maximum depth for which we tested our agents was $D_{\text{enc}} = 10$.

b. Influence of scaling parameters λ : as pointed out by Schuld *et al.* [48], for VQCs of the form of Fig. 2, expectation values of general Hermitian observables $\langle O_a \rangle_{s,\theta}$ are periodic functions of their input components s_j , with period 2π . Since the policies learned by our agents should not be periodic in general, we systematically normalize all state vectors s w.r.t. ℓ_∞ -norm (such that each normalized component \tilde{s}_i is in $[-1, 1]$) in all benchmarking environments. Additionally fixing λ to 1 does not overlook this periodicity, but rather highlights the influence of these scaling parameters on the expressivity of the VQC policies. And indeed, we observe that training these scaling parameters in general increases the learning performance of our quantum policies, especially raw-VQC policies.

c. Influence of trainable observable weights w for softmax-VQCs: our final consideration relates to the importance of having a policy with “trainable greediness” in RL scenarios. We consider softmax-VQC agents for which the observables $\langle O_a \rangle_{s,\theta}$ (see Def. 2) are kept fixed throughout training (and moreover, are equivalent to those used by their analog raw-VQC agents). We observe that this has the general effect of decreasing the performance and/or the speed of convergence of the softmax-VQC agents on all three benchmarking tasks. We further highlight the effect of properly setting the greediness of softmax policies (or, equivalently, the range of the observables $\beta \langle O_a \rangle_{s,\theta}$ used by softmax-VQCs). We do this by considering two values for their greediness parameter β (2 and 10), fixed throughout training. As a consequence, applying these softmax _{β} functions now exerts a “fixed amount of greediness”, which for high β (e.g., 10), starts approximating argmax functions commonly used by classifiers. We see that policies with fixed high β (or equivalently, a large range for their observables $\beta \langle O_a \rangle_{s,\theta}$) tend to have a poor learning performance, likely due to their lack of exploration in the RL environments.

In all our experiments, the training of the quantum agents is followed by a testing phase of 100 episodes, where the training of the agents’ policies is interrupted and β is set to 100 for softmax-VQC agents. The reason for this testing phase is twofold: first, it showcases the residual standard deviation in average learning performance due to the finite number of agents used for each curve, as well as the stochasticity of their policies; second, for softmax-VQC agents, it tests the performance of their policies when made extremely greedy. We can then observe that big shifts in performance (positive or negative) are possible simply by making trained policies more greedy, and that the average performance of the agents during training is quite representative of their true performance.

D. Shape of policies learned by VQCs v.s. NNs

The results of the last subsections demonstrate that our VQC policies can be trained to good performance in benchmarking environments. However, seeing how sensible this performance is to the particular choice of model, added to the high standard deviation we observe in most of our learning curves, makes us question the suitability of these policies to the task environments. To assess this potential mismatch, we compare the policies learned by our softmax-VQC agents on CartPole to those learned by standard DNNs (with a softmax output layer), which are known to easily learn close-to-optimal behavior on this task. More specifically, we look at the functions learned by these two models, prior to the application of the softmax normalization function (see Eq. 5). Typical instances of these functions are depicted in Figure 6, deferred to the Appendix. We observe that, while DNNs learn simple, close to piece-wise linear functions of their input state space, VQCs tend to naturally learn very oscillating functions that are more prone to instability. While the results of Schuld *et al.* [48] already indicated that these highly oscillating functions would be natural for VQCs, it is nonetheless noteworthy to see that these are also the type of functions naturally learned in RL scenarios. Moreover, our enhancements to standard VQCs show how to make these highly oscillating functions more amenable to real-world tasks.

VI. QUANTUM ADVANTAGE OF VQC AGENTS IN RL ENVIRONMENTS

The proof-of-concept experiments of the previous section show that our VQC agents can learn in standard classical environments. However, when compared to popular DNN policies trained on these tasks, our VQC policies are arguably more complex, and hence potentially not best suited for these types of environments. This observation naturally raises the question of whether there exist RL environments where the natural policies learned by VQCs can provide a learning advantage over standard classical policies. In this section, we answer this question in the affirmative by constructing: a) environments with a provable separation in learning performance between quantum and any classical (polynomial-time) learners, and b) environments where the particular VQC policies we introduced in Sec. IV show an empirical quantum advantage over standard DNN policies.

A. Quantum advantage of VQC policies over any classical learner

In this subsection, we construct RL environments with theoretical guarantees of separation between quantum and classical learning agents. These constructions are predominantly based on the recent work of Liu *et al.*

[16], which defines a classification task out of the discrete logarithm problem (DLP), i.e., the problem solved in the seminal work of Shor [38]. In broad strokes, this task can be viewed as an encryption of an easy-to-learn problem. For an “un-encrypted” version, one defines a labeling f_s of integers between 0 and $p - 2$ (for a large prime p), where the integers are labeled positively if and only if they lie in the segment $[s, s + (p-3)/2] \pmod{p-1}$. Since this labeling is linearly separable, the concept class $\{f_s\}_s$ is then easy to learn. To make it hard, the input integers x (now between 1 and $p - 1$) are encrypted using modular exponentiation, i.e., the secure operation performed in the Diffie–Hellman key exchange protocol. In the encrypted problem, the logarithm of the input integer $\log_g(x)$ (for a generator g of \mathbb{Z}_p^* , see Appendix G) hence determines the label of x . Without the ability to decrypt by solving DLP, which is widely believed to be classically intractable, the numbers appear randomly labeled. Moreover, Liu *et al.* show that achieving non-trivial labeling accuracy $1/2 + 1/\text{poly}(n)$ (for $n = \log(p)$, i.e., slightly better than random guessing) with a classical polynomial-time algorithm that uses $\text{poly}(n)$ examples would imply an efficient classical algorithm that solves DLP [16]. In contrast, the same authors construct a family of quantum learners based on Shor’s algorithm, that can achieve a labeling accuracy larger than 0.99 with high probability.

In this section, our objective is to show that analogous separations between classical and quantum learners can be established for RL environments. Specifically, we construct families of RL environments for which we can guarantee a separation in terms of the *value function* (see Sec. III A) attainable by classical versus quantum agents. Before going into detail, it is important to point out that supervised learning tasks (and so the classification problem of Liu *et al.*) can be trivially embedded into RL environments [29]: for a given concept f_s , the states x are datapoints, an action a is an agent’s guess on the label of x , an immediate reward specifies if it was correct (i.e., $f_s(x) = a$), and subsequent states are chosen uniformly at random. In such settings, the value function is straightforwardly related to the testing accuracy of the original problem yielding a simple reduction of the proof of separation of Liu *et al.* to an RL setting. This constitutes the first family of environments that we provide, and which we call SL-DLP.

In the SL-DLP construction, we made the environment fully random in order to simulate the process of obtaining i.i.d. samples in an SL setting. It is an interesting question whether similar results can be obtained for environments that are less random, and endowed with temporal correlations (i.e., such that states and actions influence subsequent states), which is characteristic of RL. In our second family of environments (Cliffwalk-DLP), we hence supplement the SL-DLP construction with next-state transitions that follow a chain-ordering of all possible states and can lead to immediate episode termination for some actions of the agent. We enforce however

that these transitions do not happen deterministically and still lead to uniformly sampled next states with a certain probability δ (common in RL to ensure that an agent is not simply memorizing a correct sequence of actions). This allows us to show that, as long as sufficient randomness is provided, it is still possible to recover a simple classical-quantum separation. We emphasize that, in the two families constructed above, each individual environment provided the randomness needed for a reduction from the SL problem.

This brings us to the question of whether separations are also possible for fully deterministic environments. In this case, it is clear that for any given environment, there exists an efficient classical agent which performs perfectly over any polynomial horizon (a lookup-table will do). However, we show in our third family of environments (Deterministic-DLP) that a separation can still be attained by moving the randomness to the choice of the environment itself: assuming an efficient classical agent which is guaranteed to be successful in most of exponentially-many randomly generated (but otherwise deterministic) environments, implies the existence of a classical efficient algorithm for DLP.

We summarize our results in the following Theorem, detailed and proven in Appendix H.

Theorem 2. *There exist families of reinforcement learning environments which are: i) fully random (i.e., subsequent states are independent from the previous state and action); ii) partially random (i.e., the previous moves determine subsequent states, except with a probability δ at least 0.86 where they are chosen uniformly at random), and iii) fully deterministic; such that there exists a separation in the value functions achievable by a given quantum polynomial-time agent and any classical polynomial-time agent. Specifically, the value of the initial state for the quantum agent $V_q(s_0)$ is ε -close to the optimal value function (for a chosen ε , and with probability above 2/3). Further, if there exists a classical efficient learning agent that achieves a value $V_c(s_0)$ better than $V_{\text{rand}}(s_0) + \varepsilon'$ (for a chosen ε' , and with probability above 0.845), then there exists a classical efficient algorithm to solve DLP. Finally, we have $V_q(s_0) - V_c(s_0)$ larger than some constant, which depends on the details of the environment.*

We believe that this result can be generalized further to even wider classes of RL environments, and in particular that the parameter δ in the partially-random environments can likely be made unlimited, by combining our approaches in *ii*) and *iii*). However, in the remainder of this work, we want to focus on two other issues. The first pertains to the special form of the environments, which are based on algebraic properties that confer explicit *meaning* to the labels and that learning agents must exploit. As for the second issue, it concerns the agents we rely on, which do not learn by sequentially adapting their policy as is natural in RL, but through a supervised method tailored to the problems, namely, quantum support vector machines (SVMs) [10, 11].

We start by addressing this second issue. For that, we note that relying on learning agents that use direct kernel methods is not necessary to achieve close-to-optimal performance on the DLP environments. Instead, we can design agents that use a “more sequential” approach to learning, based on steepest-ascent updates of a VQC policy, and still achieve a similar performance. To understand this distinction and how it can be circumvented, we remind the reader of the two models for quantum SVMs defined in Ref. [10]: the explicit and the implicit model. In the implicit model one first computes the kernel

$$K(x_i, x_j) = |\langle \phi(x_i) | \phi(x_j) \rangle|^2 \quad (10)$$

for the feature states $|\phi(x)\rangle$ associated to each pair of data points $\{x_i, x_j\}$ in the dataset, which is then processed by a classical SVM algorithm to compute a hyperplane classifier \mathbf{w} . In the explicit model, the classifier is obtained by variationally training in feature space an approximate normal vector $|\mathbf{w}^\perp\rangle$ to this separating hyperplane. The projector associated to this normal vector can be directly measured on the feature states $|\phi(x)\rangle$ such that the sign of $|\langle \mathbf{w}^\perp | \phi(x) \rangle|^2 + b$, for a bias b , gives the label of x . The latter model is more restrictive in the sense that it can not represent all hyperplanes (each hyperplane is defined by its corresponding observable, and these observables are limited by the variational part of the circuit). However, the advantage for our purposes is that this latter model is trainable in the same way as our VQC agents.

It is not difficult to construct a family of VQC classifiers which is as powerful in the DLP environments as the implicit quantum SVMs of Liu *et al.* Take a VQC using the same feature embedding $|\phi(x)\rangle$ as the one specifying their kernel, and a variational part that parametrizes all the meaningful hyperplanes in this feature space (see Appendix K for details of this construction). This VQC classifier has then the capacity of representing all optimal policies in the DLP environments. Moreover, we show that, even under similar noise considerations as Liu *et al.*, this optimal classifier can be found using $\text{poly}(n)$ random data samples (see Appendix L for the proof). However, it is still an open question if such a method can be combined with batch-learning of the type we have in RL while keeping the same performance guarantees. For this, care must be taken such that the optimization process does not end up in a local minimum.

But again, such a VQC model, even when completely worked out, would not be fully satisfactory due to the very tailored nature of both the feature map and the variational model it relies on. Indeed, these exploit Shor’s algorithm to perform a very explicit decryption of the input states, which renders learning easy (the problem becomes linearly separable). Instead, we would like to consider abstract environments that are less tailored to a specific decryption function, which would allow more general agents to learn. We hence consider next environments which are themselves defined using VQCs, such that quantum agents *could* learn them efficiently, yet

classical agents are likely to fail (assuming the VQC functions used to generate the environment are hard to simulate classically). We emphasize that constructing an environment such that optimal and trained policies belong to the same family of VQCs certainly does not guarantee that the former will be learned efficiently. Equally, the fact that the environment is based on a classically-hard function does not trivially mean that a classical model can not learn it, especially in the case of limited problem size n (i.e. non-asymptotic cases). We manage to show however, in numerical experiments, that such environments which exhibit both quantum learnability by VQC agents and hardness of learning for standard classical policies do exist.

B. Quantum advantage of VQC policies over DNN policies

1. VQC-generated environments

In their seminal work on quantum kernel methods, Havlíček *et al.* [10] describe a VQC classifier composed of a feature-encoding unitary (the analog of our data-encoding unitaries) followed by a variational unitary and the measurement of a $Z^{\otimes n}$ expectation value. To test the performance of their model, they design a classification task where the labeling function (or ground truth) itself is generated by a similar classifier. More specifically, this generating classifier uses the same feature-encoding unitary, but followed by a fixed random unitary sampled from $\text{SU}(2)$ (and the same $Z^{\otimes n}$ measurement). They show that, on this classification task, their VQC classifier achieves close-to-optimal performance. Due to the conjectured hardness of simulating their feature-encoding, this result hence suggests that this task should also be intractable for classical learners, for large n .

In this work, we take a similar approach to that of [10], in which we generate RL environments out of random raw-VQC policies. We detail the construction of these environments below. First, we fix a raw-VQC policy that uses the alternating-layer architecture of Fig. 2, acts on $n = 2$ qubits, with depth $D_{\text{enc}} = 4$ and uniformly sampled parameters $\boldsymbol{\theta}$. We then generate a labeling function by assigning a label $+1$ to the datapoints s in $[0, 2\pi]^2$ for which $\langle ZZ \rangle_{s, \boldsymbol{\theta}} \geq 0$ and a label -1 otherwise. We then generate a dataset S of 10 datapoints per label, by uniformly sampling points in $[0, 2\pi]^2$ that are $\frac{\Delta}{2} = 0.15$ away from the margin of the labeling function, i.e., for which $|\langle ZZ \rangle_{s, \boldsymbol{\theta}}| \geq \frac{\Delta}{2}$. This dataset allows us to define two RL environments on which we can test the performance of softmax-VQC and DNN agents:

- SL-VQC environment: similarly to the SL-DLP construction of Sec. VI A, we first define a degenerate RL environment, in the sense that it simply encodes an SL task in a multi-step RL environment. An episode of interaction goes as follows: at each interaction step, a

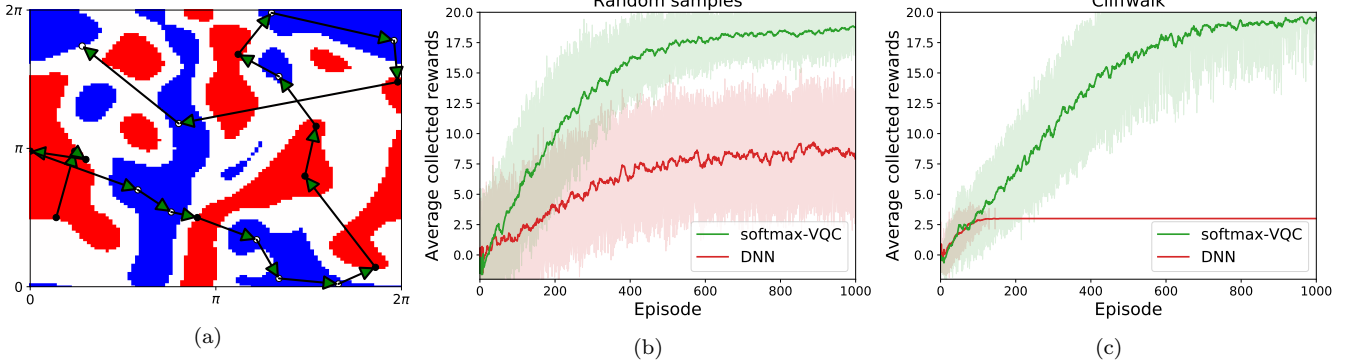


Figure 5. Numerical evidence of the advantage of VQC policies over NN policies in VQC-generated environments. (a) Labeling function and training data used for both RL environments. The data labels (red for $+1$ label and blue for -1 label) are generated using a raw-VQC of depth $D_{\text{enc}} = 4$ with a margin $\Delta = 0.3$ (white areas). The training samples (10 datapoints per label) are uniformly sampled from the blue and red regions. The arrows indicate the rewarded path of the cliffwalk environment used in (c). (b) and (c) The learning curves (20 agents per curve) of randomly-initialized softmax-VQC agents and DNN agents in two RL environments generated by the VQC labeling function, where input states are (b) uniformly sampled from the dataset and (c) follow cliffwalk dynamics. Each curve is temporally averaged with a time window of 10 episodes. The VQC architecture of the softmax-VQC agents is the same as that of the raw-VQC generating the labeling function (they differ however in their (uniformly random) parameter initialization). The DNNs have 4 hidden layers of 16 Rectified Linear Units (ReLUs) each, followed by a softmax output layer of size 2.

sample state s is uniformly sampled from the dataset S , the agent then acts with a label $+1/-1$ and a $+1$ (-1) reward is issued by the environment when the sample has been correctly (incorrectly) classified by the agent. The episode has a fixed length (or horizon H) of 20 interactions.

- Cliffwalk-VQC environment: again, in order to get an environment that is closer to “true” RL in nature, we define a second environment similar to the Cliffwalk-DLP environment of Sec. VI A (except that it’s now deterministic), and inspired by the textbook “cliff walking” environment of Sutton & Barto [25]. This environment basically keeps the same action and reward structure of the SL-VQC environment but adds a temporal structure to it: each episode starts from a fixed state $s_0 \in S$, and if an agent assigns the correct label to a state s_i , $0 \leq i \leq 19$, it moves to a fixed state s_{i+1} and receives a $+1$ reward, otherwise the episode is instantly terminated and the agent receives a -1 reward. We set s_{20} to be a termination state such that each episode has a maximum length $H = 20$ interactions.

2. Performance comparison

Having defined our VQC-generated environments, we now evaluate the performance of softmax-VQC and DNN policies on these tasks. The particular models we consider are softmax-VQCs with VQCs sampled from the same family as that of the raw-VQCs generating the environments (but with different randomly initialized parameters θ), and DNNs with Rectified Linear Units (ReLUs) in their hidden layers. In our hyperparameter search, we

evaluate the performance of DNNs with a wide range of depths (number of hidden layers between 2 to 10) and widths (number of units per hidden layer between 8 and 64), and keep the architecture with the best average performance (depth 4, width 16).

Despite this hyperparametrization, we find (see Fig. 5, and Fig. 7 in the Appendix for different instances of the environments) that the performance of DNN policies on these tasks remains limited compared to that of softmax-VQCs, that reach close-to-optimal performance on both tasks. Moreover, we observe that the separation between the performance of both models gets boosted by the cliffwalk temporal structure. This can be explained by the increased complexity of this task, as, in order to move farther in the cliffwalk, the policy family should allow learning new labels without “forgetting” the labels of earlier states. This hence requires enough flexibility in the policy family to change assigned labels only *locally* on the state space. It appears then that the softmax-VQC policies have this inherent flexibility, while DNNs do not. We confirm this intuition by having a closer look at the policies learned by DNNs and softmax-VQCs, depicted in Fig. 8 of the Appendix. We indeed observe that the typical policies learned by DNNs are rather simple, with up to 2 (or 3) regions, delimited by close-to-linear boundaries, as opposed to the policies learned by softmax-VQCs, which delimit red from blue regions with wide margins.

3. Outlook

In order to strengthen the claim of classical hardness of these environments, we could consider different gener-

ating circuits in place of our alternating-layered VQCs. Instead of these, we would define a family of unitaries which guarantees that the expectation value of some observable is classically hard to estimate. Such unitaries, with the additional constraint that they should have constant depth for near-term implementation, are challenging to find. Indeed, efficient classical algorithms for estimating quantum expectation values of constant depth circuits are known [52] (for local 2D qubit connectivity and/or restricted structures of observables). To get around these limitations, one could consider architectures with more general connectivity, or greater depth, e.g., logarithmic in the number of qubits [53–55].

VII. CONCLUSION AND OUTLOOK

In this work, we have investigated the design of quantum RL agents based on VQCs. We explored a selection of VQC models and showed, through numerical simulations, the impact of certain design choices on learning performance. In particular, we introduced the softmax-VQC model, where one computes a softmax policy using expectation values of a VQC with both trainable observables and input scaling parameters. These added features to standard VQCs used in ML (e.g., as quantum classifiers), enhance both the expressivity and flexibility of VQC policies, by enriching their Fourier spectrum [48] and allowing easier shifts between exploration and exploitation. In turn, this allows our quantum agents to achieve a learning performance on classical benchmarking environments that is comparable to that of standard DNNs used in deep RL. We found however that these task environments, while being very natural for DNNs, are mismatched to VQCs, due to the particular “oscillating type” of functions that are naturally represented by a large class of VQC models for ML. Conversely, we demonstrated the existence of task environments, constructed out of VQC functions, that are very natural for VQC agents, but on which DNN agents have a poor performance. This constitutes a first numerical evidence of a quantum advantage of VQC policies in classical RL environments. To strengthen this result, we constructed several RL environments, each with a different degree of degeneracy (i.e., closeness to a supervised learning task), where we showed a rigorous separation between a class of VQC agents and any classical learner, based on the widely-believed classical hardness of the discrete logarithm problem. Our numerical investigation also indicates that RL is an interesting numerical test-bed to compare VQC models for ML (or QML models in general), since it boosts separations in performance compared to supervised learning tasks. This makes it easier to compare models that are small in size, as the RL setting will result in bigger separations, which is ideal for near-term experiments. In conclusion, we believe that our results constitute strides toward a

practical quantum advantage in RL using near-term quantum devices.

Regarding follow-up work, it would be interesting to test the impact of the VQC features we introduced (i.e., trainable observables and input scaling parameters) in a more general ML setting. We believe that these enhancements would also benefit other VQC models, such as VQC classifiers and function approximators. It would also be worthwhile to explore more elaborate policy gradient methods [42] such as an actor-critic approach, and especially the natural actor-critic formulation with compatible function approximation [56], where one could exploit the method of Stokes *et al.* [57] to compute quantum natural gradients. One could consider as well exploring more specific initialization strategies for the parameters of our VQCs as a way to improve their performance (which was investigated in great detail for DNNs [58, 59]). In light of our numerical results, parameter initialization could be a potential solution to learn VQC functions that are nicely behaving, or at least reduce the variance in performance between different randomly initialized agents. Assessing this performance under errors of approximation and noise considerations (or on actual quantum devices) would also constitute an interesting direction. Finally, in consideration of the recent results on barren plateaus in the optimization landscape of VQCs [23, 24], one could try to determine the impact (positive or negative) of both trainable observables and the policy-dependent cost function that is a value function on these optimization landscapes.

ACKNOWLEDGMENTS

The authors would like to thank Srinivasan Arunachalam for clarifications on the testing accuracy of their quantum classifier in the DLP classification task. The authors would also like to thank Andrea Skolik and Arjan Cornelissen for helpful discussions and comments. CG thanks Thomas Moerland for discussions in the early phases of this project. SJ and HJB acknowledge support from the Austrian Science Fund (FWF) through the projects DK-ALM:W1259-N27 and SFB BeyondC F7102. SJ also acknowledges the Austrian Academy of Sciences as a recipient of the DOC Fellowship. This work was in part supported by the Dutch Research Council (NWO/OCW), as part of the Quantum Software Consortium program (project number 024.003.037). VD and SM acknowledge the support by the project NEASQC funded from the European Union’s Horizon 2020 research and innovation programme (grant agreement No 951821). VD and SM also acknowledge partial funding by an unrestricted gift from Google Quantum AI. The computational results presented here have been achieved in part using the LEO HPC infrastructure of the University of Innsbruck.

[1] J. Preskill, Quantum computing in the nisq era and beyond, *Quantum* **2**, 79 (2018).

[2] K. Bharti, A. Cervera-Lierta, T. H. Kyaw, T. Haug, S. Alperin-Lea, A. Anand, M. Degroote, H. Heimonen, J. S. Kottmann, T. Menke, *et al.*, Noisy intermediate-scale quantum (nisq) algorithms, arXiv preprint arXiv:2101.08448 (2021).

[3] M. Cerezo, A. Arrasmith, R. Babbush, S. C. Benjamin, S. Endo, K. Fujii, J. R. McClean, K. Mitarai, X. Yuan, L. Cincio, *et al.*, Variational quantum algorithms, arXiv preprint arXiv:2012.09265 (2020).

[4] F. Arute, K. Arya, R. Babbush, D. Bacon, J. C. Bardin, R. Barends, R. Biswas, S. Boixo, F. G. Brandao, D. A. Buell, *et al.*, Quantum supremacy using a programmable superconducting processor, *Nature* **574**, 505 (2019).

[5] H.-S. Zhong, H. Wang, Y.-H. Deng, M.-C. Chen, L.-C. Peng, Y.-H. Luo, J. Qin, D. Wu, X. Ding, Y. Hu, *et al.*, Quantum computational advantage using photons, *Science* **370**, 1460 (2020).

[6] M. Benedetti, E. Lloyd, S. Sack, and M. Fiorentini, Parameterized quantum circuits as machine learning models, *Quantum Science and Technology* **4**, 043001 (2019).

[7] N. Killoran, T. R. Bromley, J. M. Arrazola, M. Schuld, N. Quesada, and S. Lloyd, Continuous-variable quantum neural networks, *Physical Review Research* **1**, 033063 (2019).

[8] E. Farhi and H. Neven, Classification with quantum neural networks on near term processors, arXiv preprint arXiv:1802.06002 (2018).

[9] M. Schuld, A. Bocharov, K. M. Svore, and N. Wiebe, Circuit-centric quantum classifiers, *Physical Review A* **101**, 032308 (2020).

[10] V. Havlíček, A. D. Córcoles, K. Temme, A. W. Harrow, A. Kandala, J. M. Chow, and J. M. Gambetta, Supervised learning with quantum-enhanced feature spaces, *Nature* **567**, 209 (2019).

[11] M. Schuld and N. Killoran, Quantum machine learning in feature hilbert spaces, *Physical review letters* **122**, 040504 (2019).

[12] J.-G. Liu and L. Wang, Differentiable learning of quantum circuit born machines, *Physical Review A* **98**, 062324 (2018).

[13] D. Zhu, N. M. Linke, M. Benedetti, K. A. Landsman, N. H. Nguyen, C. H. Alderete, A. Perdomo-Ortiz, N. Korda, A. Garfoot, C. Brecque, *et al.*, Training of quantum circuits on a hybrid quantum computer, *Science advances* **5**, eaaw9918 (2019).

[14] J. Otterbach, R. Manenti, N. Alidoust, A. Bestwick, M. Block, B. Bloom, S. Caldwell, N. Didier, E. S. Fried, S. Hong, *et al.*, Unsupervised machine learning on a hybrid quantum computer, arXiv preprint arXiv:1712.05771 (2017).

[15] Y. Du, M.-H. Hsieh, T. Liu, and D. Tao, Expressive power of parametrized quantum circuits, *Physical Review Research* **2**, 033125 (2020).

[16] Y. Liu, S. Arunachalam, and K. Temme, A rigorous and robust quantum speed-up in supervised machine learning, arXiv preprint arXiv:2010.02174 (2020).

[17] H.-Y. Huang, M. Broughton, M. Mohseni, R. Babbush, S. Boixo, H. Neven, and J. R. McClean, Power of data in quantum machine learning, arXiv preprint arXiv:2011.01938 (2020).

[18] M. Schuld, R. Swoke, and J. J. Meyer, The effect of data encoding on the expressive power of variational quantum machine learning models, arXiv preprint arXiv:2008.08605 (2020).

[19] A. Abbas, D. Sutter, C. Zoufal, A. Lucchi, A. Figalli, and S. Woerner, The power of quantum neural networks, arXiv preprint arXiv:2011.00027 (2020).

[20] P. Huembeli and A. Dauphin, Characterizing the loss landscape of variational quantum circuits, arXiv preprint arXiv:2008.02785 (2020).

[21] A. Skolik, J. R. McClean, M. Mohseni, P. van der Smagt, and M. Leib, Layerwise learning for quantum neural networks, *Quantum Machine Intelligence* **3**, 1 (2021).

[22] Z. Holmes, K. Sharma, M. Cerezo, and P. J. Coles, Connecting ansatz expressibility to gradient magnitudes and barren plateaus, arXiv preprint arXiv:2101.02138 (2021).

[23] J. R. McClean, S. Boixo, V. N. Smelyanskiy, R. Babbush, and H. Neven, Barren plateaus in quantum neural network training landscapes, *Nature communications* **9**, 1 (2018).

[24] M. Cerezo, A. Sone, T. Volkoff, L. Cincio, and P. J. Coles, Cost-function-dependent barren plateaus in shallow quantum neural networks, arXiv preprint arXiv:2001.00550 (2020).

[25] R. S. Sutton, A. G. Barto, *et al.*, *Reinforcement learning: An introduction* (1998).

[26] V. Dunjko, J. M. Taylor, and H. J. Briegel, Advances in quantum reinforcement learning, in *2017 IEEE International Conference on Systems, Man, and Cybernetics (SMC)* (IEEE, 2017) pp. 282–287.

[27] G. D. Paparo, V. Dunjko, A. Makmal, M. A. Martin-Delgado, and H. J. Briegel, Quantum speedup for active learning agents, *Physical Review X* **4**, 031002 (2014).

[28] V. Dunjko, J. M. Taylor, and H. J. Briegel, Quantum-enhanced machine learning, *Physical review letters* **117**, 130501 (2016).

[29] V. Dunjko, Y.-K. Liu, X. Wu, and J. M. Taylor, Exponential improvements for quantum-accessible reinforcement learning, arXiv preprint arXiv:1710.11160 (2017).

[30] F. Neukart, D. Von Dollen, C. Seidel, and G. Compostella, Quantum-enhanced reinforcement learning for finite-episode games with discrete state spaces, *Frontiers in Physics* **5**, 71 (2018).

[31] S. Y.-C. Chen, C.-H. H. Yang, J. Qi, P.-Y. Chen, X. Ma, and H.-S. Goan, Variational quantum circuits for deep reinforcement learning, *IEEE Access* **8**, 141007 (2020).

[32] O. Lockwood and M. Si, Reinforcement learning with quantum variational circuit, in *Proceedings of the AAAI Conference on Artificial Intelligence and Interactive Digital Entertainment*, Vol. 16 (2020) pp. 245–251.

[33] S. Wu, S. Jin, D. Wen, and X. Wang, Quantum reinforcement learning in continuous action space, arXiv preprint arXiv:2012.10711 (2020).

[34] S. Jerbi, L. M. Trenkwalder, H. Poulsen Nautrup, H. J. Briegel, and V. Dunjko, Quantum enhancements for deep reinforcement learning in large spaces, *PRX Quantum* **2**, 010328 (2021).

[35] D. Silver, J. Schrittwieser, K. Simonyan, I. Antonoglou, A. Huang, A. Guez, T. Hubert, L. Baker, M. Lai, A. Bolton, *et al.*, Mastering the game of go without hu-

man knowledge, *Nature* **550**, 354 (2017).

[36] R. S. Sutton, D. A. McAllester, S. P. Singh, and Y. Mansour, Policy gradient methods for reinforcement learning with function approximation, in *Advances in neural information processing systems* (2000) pp. 1057–1063.

[37] V. R. Konda and J. N. Tsitsiklis, Actor-critic algorithms, in *Proceedings of the 12th International Conference on Neural Information Processing Systems* (1999) pp. 1008–1014.

[38] P. W. Shor, Polynomial-time algorithms for prime factorization and discrete logarithms on a quantum computer, *SIAM review* **41**, 303 (1999).

[39] S. M. Kakade, *On the sample complexity of reinforcement learning*, Ph.D. thesis, UCL (University College London) (2003).

[40] D. Silver, Lectures on reinforcement learning, URL: <https://www.davidsilver.uk/teaching/> (2015).

[41] R. J. Williams, Simple statistical gradient-following algorithms for connectionist reinforcement learning, *Machine learning* **8**, 229 (1992).

[42] L. Weng, Policy gradient algorithms, URL: <https://lilianweng.github.io/lil-log> (2018).

[43] E. Greensmith, P. L. Bartlett, and J. Baxter, Variance reduction techniques for gradient estimates in reinforcement learning, *Journal of Machine Learning Research* **5**, 1471 (2004).

[44] T. Jie and P. Abbeel, On a connection between importance sampling and the likelihood ratio policy gradient, *Advances in Neural Information Processing Systems* **23**, 1000 (2010).

[45] Y. Duan, X. Chen, R. Houthooft, J. Schulman, and P. Abbeel, Benchmarking deep reinforcement learning for continuous control, in *International conference on machine learning* (PMLR, 2016) pp. 1329–1338.

[46] A. Kandala, A. Mezzacapo, K. Temme, M. Takita, M. Brink, J. M. Chow, and J. M. Gambetta, Hardware-efficient variational quantum eigensolver for small molecules and quantum magnets, *Nature* **549**, 242 (2017).

[47] A. Pérez-Salinas, A. Cervera-Lierta, E. Gil-Fuster, and J. I. Latorre, Data re-uploading for a universal quantum classifier, *Quantum* **4**, 226 (2020).

[48] M. Schuld, V. Bergholm, C. Gogolin, J. Izaac, and N. Killoran, Evaluating analytic gradients on quantum hardware, *Physical Review A* **99**, 032331 (2019).

[49] K. Mitarai, M. Negoro, M. Kitagawa, and K. Fujii, Quantum circuit learning, *Physical Review A* **98**, 032309 (2018).

[50] G. Brockman, V. Cheung, L. Pettersson, J. Schneider, J. Schulman, J. Tang, and W. Zaremba, Openai gym, arXiv preprint arXiv:1606.01540 (2016).

[51] OpenAI, Leaderboard of openai gym environments, GitHub, <https://github.com/openai/gym/wiki/Leaderboard> (2020).

[52] S. Bravyi, D. Gosset, and R. Movassagh, Classical algorithms for quantum mean values, *Nature Physics* **1**, 1 (2021).

[53] R. Cleve and J. Watrous, Fast parallel circuits for the quantum fourier transform, in *Proceedings 41st Annual Symposium on Foundations of Computer Science* (IEEE, 2000) pp. 526–536.

[54] C. Moore and M. Nilsson, Parallel quantum computation and quantum codes, *SIAM Journal on Computing* **31**, 799 (2001).

[55] G. Evenbly and G. Vidal, Algorithms for entanglement renormalization, *Physical Review B* **79**, 144108 (2009).

[56] J. Peters, S. Vijayakumar, and S. Schaal, Natural actor-critic, in *European Conference on Machine Learning* (Springer, 2005) pp. 280–291.

[57] J. Stokes, J. Izaac, N. Killoran, and G. Carleo, Quantum natural gradient, *Quantum* **4**, 269 (2020).

[58] X. Glorot and Y. Bengio, Understanding the difficulty of training deep feedforward neural networks, in *Proceedings of the thirteenth international conference on artificial intelligence and statistics* (JMLR Workshop and Conference Proceedings, 2010) pp. 249–256.

[59] K. He, X. Zhang, S. Ren, and J. Sun, Delving deep into rectifiers: Surpassing human-level performance on imagenet classification, in *Proceedings of the IEEE international conference on computer vision* (2015) pp. 1026–1034.

[60] H. H. Ku *et al.*, Notes on the use of propagation of error formulas, *Journal of Research of the National Bureau of Standards* **70**, 263 (1966).

[61] Google, Cirq: A python framework for creating, editing, and invoking noisy intermediate scale quantum circuits, URL: <https://github.com/quantumlib/Cirq> (2018).

[62] Y. Suzuki, Y. Kawase, Y. Masumura, Y. Hiraga, M. Nakadai, J. Chen, K. M. Nakanishi, K. Mitarai, R. Imai, S. Tamiya, *et al.*, Qulacs: a fast and versatile quantum circuit simulator for research purpose, arXiv preprint arXiv:2011.13524 (2020).

Appendix A: Derivation of the log-policy gradient

For a softmax-VQC defined in Def. 2, we have:

$$\begin{aligned} \nabla_{\boldsymbol{\theta}} \log \pi_{\boldsymbol{\theta}}(a|s) &= \nabla_{\boldsymbol{\theta}} \log e^{\beta \langle O_a \rangle_{s, \boldsymbol{\theta}}} - \nabla_{\boldsymbol{\theta}} \log \sum_{a'} e^{\beta \langle O_{a'} \rangle_{s, \boldsymbol{\theta}}} \\ &= \beta \nabla_{\boldsymbol{\theta}} \langle O_a \rangle_{s, \boldsymbol{\theta}} - \sum_{a'} \frac{e^{\beta \langle O_{a'} \rangle_{s, \boldsymbol{\theta}}} \beta \nabla_{\boldsymbol{\theta}} \langle O_{a'} \rangle_{s, \boldsymbol{\theta}}}{\sum_{a''} e^{\beta \langle O_{a''} \rangle_{s, \boldsymbol{\theta}}}} \\ &= \beta \left(\nabla_{\boldsymbol{\theta}} \langle O_a \rangle_{s, \boldsymbol{\theta}} - \sum_{a'} \pi_{\boldsymbol{\theta}}(a'|s) \nabla_{\boldsymbol{\theta}} \langle O_{a'} \rangle_{s, \boldsymbol{\theta}} \right). \end{aligned}$$

Appendix B: Efficient approximate policy sampling

Consider $|A|$ independent estimates $\left\{ \widetilde{\langle O_i \rangle}_{s, \boldsymbol{\theta}} \right\}_{|A|}$, obtained to additive error ε_i , respectively. These estimates are used to compute an approximate policy $\widetilde{\pi}_{\boldsymbol{\theta}}$, using Eq. (5) (in the following, w.l.o.g., we absorb β in all the observables O_i). We want to derive a bound on the total variation distance between $\widetilde{\pi}_{\boldsymbol{\theta}}$ and the true $\pi_{\boldsymbol{\theta}}$, as a function of ε_i . For that, we rely on the following error propagation formulas [60]:

- (i) $C = ae^{bA} \Rightarrow \mathcal{E}(C) \approx C|b|\mathcal{E}(A)$
- (ii) $C = aA + bB \Rightarrow \mathcal{E}(C) = \sqrt{a^2\mathcal{E}(A)^2 + b^2\mathcal{E}(B)^2}$
- (iii) $C = \frac{A}{B} \Rightarrow \mathcal{E}(C) \approx C \sqrt{\frac{\mathcal{E}(A)^2}{A^2} + \frac{\mathcal{E}(B)^2}{B^2} - 2\frac{\mathcal{E}(A, B)^2}{AB}}$

for random variables A, B, C and real constants a, b , where A and B are assumed independent in (ii) but not in (iii) ($\mathcal{E}(A, B)$ is the covariance of A and B).

Using these formulas, we get:

$$\begin{aligned}\mathcal{E}\left(e^{-\langle\widetilde{O}_i\rangle_{s,\theta}}\right) &\approx e^{-\langle\widetilde{O}_i\rangle_{s,\theta}}\varepsilon_i \\ \mathcal{E}\left(\sum_j e^{-\langle\widetilde{O}_j\rangle_{s,\theta}}\right) &\lesssim \sum_j e^{-\langle\widetilde{O}_j\rangle_{s,\theta}}\varepsilon_i\end{aligned}$$

by repeated applications of formula (ii) and the triangular inequality. Then, for $\tilde{\pi}_{\theta}(i) = \frac{e^{-\langle\widetilde{O}_i\rangle_{s,\theta}}}{\sum_j e^{-\langle\widetilde{O}_j\rangle_{s,\theta}}}$:

$$\begin{aligned}\mathcal{E}(\tilde{\pi}_{\theta}(i)) &\approx \tilde{\pi}_{\theta}(i) \sqrt{\varepsilon_i^2 + \frac{\left(\sum_j e^{-\langle\widetilde{O}_j\rangle_{s,\theta}}\varepsilon_j\right)^2}{\left(\sum_j e^{-\langle\widetilde{O}_j\rangle_{s,\theta}}\right)^2} - 2\tilde{\pi}_{\theta}(i)\varepsilon_i^2} \\ &\leq \tilde{\pi}_{\theta}(i)\sqrt{2\varepsilon},\end{aligned}$$

by assuming $\varepsilon_i = \varepsilon, \forall i$.

Finally, we have that:

$$\begin{aligned}\text{TV}(\pi_{\theta}, \tilde{\pi}_{\theta}) &= \sum_i |\tilde{\pi}_{\theta}(i) - \pi_{\theta}(i)| \\ &\leq \sum_i \frac{e^{-\langle\widetilde{O}_i\rangle_{s,\theta}}}{\sum_j e^{-\langle\widetilde{O}_j\rangle_{s,\theta}}} \sqrt{2\varepsilon} = \sqrt{2\varepsilon}.\end{aligned}$$

This proves Lemma 2.

Appendix C: Efficient estimation of the log-policy gradient

Similarly to the approach of the previous Appendix, we use error propagation formulas to bound the error on derivatives of the log-policy $\partial_i \log \pi_{\theta}(a|s)$ estimated using $\sqrt{2\varepsilon}$ -precise (to relative error) estimates of $\pi_{\theta}(a|s)$, $\forall a$, and ε' -precise (to additive error) estimates of $\partial_i \langle O_a \rangle_{s,\theta}$, $\forall a$. We rely here on a forth formula [60]:

$$(iv) \quad C = AB \Rightarrow \mathcal{E}(C) \approx C \sqrt{\frac{\mathcal{E}(A)^2}{A^2} + \frac{\mathcal{E}(B)^2}{B^2}}$$

for independent random variables A and B .

Using this formula, we get:

$$\begin{aligned}\mathcal{E}\left(\tilde{\pi}_{\theta}(a'|s)\partial_i \langle \widetilde{O}_{a'} \rangle\right) &\approx \tilde{\pi}_{\theta}(a'|s)\partial_i \langle \widetilde{O}_{a'} \rangle \sqrt{2\varepsilon^2 + \frac{\varepsilon'^2}{\partial_i \langle \widetilde{O}_{a'} \rangle^2}} \\ &\leq \tilde{\pi}_{\theta}(a'|s) \left(\partial_i \langle \widetilde{O}_{a'} \rangle \sqrt{2\varepsilon} + \varepsilon'\right),\end{aligned}$$

using the triangular inequality.

Hence, for

$$\partial_i \log \widetilde{\pi}_{\theta}(a|s) = \partial_i \langle \widetilde{O}_a \rangle_{s,\theta} - \sum_{a'} \widetilde{\pi}_{\theta}(a'|s) \partial_i \langle \widetilde{O}_{a'} \rangle_{s,\theta},$$

we have:

$$\begin{aligned}\mathcal{E}(\partial_i \log \widetilde{\pi}_{\theta}(a|s)) &\leq \sqrt{2\varepsilon} \max_a \partial_i \langle \widetilde{O}_a \rangle + 2\varepsilon' \\ &\leq \sqrt{2\varepsilon} \max_a \|\widetilde{O}_a\| + 2\varepsilon',\end{aligned}$$

where the last inequality results from the parameter-shift rule (Eq. (7)) formulation of $\partial_i \langle O_a \rangle$ for derivatives w.r.t. rotation angles of the circuit and that $\partial_i \langle O_a \rangle$ are simply expectation values themselves for observable weights.

Therefore, in order to estimate the gradient of the log-policy $\nabla_{\theta} \log \pi_{\theta}(a|s)$ up to additive error ε in ℓ_{∞} -norm, it is sufficient to estimate $\langle O_a \rangle_{s,\theta}$ to additive precision $\varepsilon(\sqrt{2}\|O_a\|)^{-1}$, $\forall a$, and $\partial_i \langle O_a \rangle_{s,\theta}$ to additive precision $\varepsilon/2$, $\forall i, a$.

Appendix D: Environments specifications

In Table I, we present a specification of the environments we consider in our numerical simulations. These are standard benchmarking environments from the OpenAI Gym library [50], described in Ref. [51], and VQC-generated environments that we define in Sec. VI B.

Appendix E: Hyperparameters

In Tables II and III, we list the hyperparameters used to train our agents on the various environments we consider. All quantum circuits were implemented using the Cirq library [61] in Python and simulated using a Qulacs backend [62] in C++. All agents use an ADAM optimizer.

Appendix F: VQC-NN policies comparison

Fig. 6 compares the policies learned by a softmax-VQC agent and a DNN agent in CartPole-v1. Fig. 7 shows the analog results to Fig. 5 but with two different random initializations of the environment-generating VQC. Fig. 8 compares the policies learned by a softmax-VQC agent and a DNN agent in one instance of these VQC-generated environments.

Appendix G: Supervised learning task of Liu *et al.*

Define p a large prime number, $n = \lceil \log_2(p-1) \rceil$, and g a generator of $\mathbb{Z}_p^* = \{1, 2, \dots, p-1\}$ (i.e., a $g \in \mathbb{Z}_p^*$ such that $\{g^x, x \in \mathbb{Z}_{p-1}\} = \mathbb{Z}_p^*$). The DLP consists in computing $\log_g x$ on input $x \in \mathbb{Z}_p^*$. Based on DLP, Liu *et al.* [16] define a concept class $\mathcal{C} = \{f_s\}_{s \in \mathbb{Z}_p^*}$ over the input space $\mathcal{X} = \mathbb{Z}_p^*$, where each labeling function of this concept class is defined as follows:

$$f_s(x) = \begin{cases} +1, & \text{if } \log_g x \in [s, s + \frac{p-3}{2}], \\ -1, & \text{otherwise.} \end{cases} \quad (\text{G1})$$

Environment	State dimension	Number of actions	Horizon	Reward function	Termination conditions
CartPole-v1	4	2	500	+1 until termination	<ul style="list-style-type: none"> Pole angle or cart position outside of bounds Reaching horizon
MountainCar-v0	2	3	200	$-1 + \text{height}$ until termination	Reaching goal or horizon
Acrobot-v1	6	3	500	-1 until termination	Reaching goal or horizon
SL-VQC	2	2	20	+1 for good action -1 for wrong action	Reaching horizon
Cliffwalk-VQC	2	2	20	+1 for good action -1 for wrong action	<ul style="list-style-type: none"> Doing wrong action Reaching horizon

Table I. **Environments specifications.** The reward function of Mountaincar-v0 has been modified compared to the standard specification of OpenAI Gym [50], similarly to Ref. [45].

Environment	Model	Learning rates	Discount γ	Final β	Batch size	Depth	Width
CartPole-v1	softmax-VQC	[0.01, 0.1, 0.1]	1	1	10	{1, 5}	4
	raw-VQC	[0.01, 0., 0.1]	1	\times	10	{1, 5}	4
MountainCar-v0	softmax-VQC	[0.01, 0.1, 0.01]	1	1.5	10	{4, 6}	2
	raw-VQC	[0.01, 0., 0.01]	1	\times	10	{4, 6}	2
Acrobot-v1	softmax-VQC	[0.01, 0.1, 0.1]	1	1	10	{2, 5}	6
	raw-VQC	[0.01, 0., 0.1]	1	\times	10	{2, 5}	6
SL-VQC	softmax-VQC	[0.01, 0.1, 0.01]	0.9	1	10	4	2
	DNN	0.01	0.9	1	10	4	16
Cliffwalk-VQC	softmax-VQC	[0.01, 0.1, 0.1]	0.9	1	10	4	2
	DNN	0.01	0.9	1	10	4	16

Table II. **Hyperparameters 1/2.** For VQC policies, we choose 3 distinct learning rates $[\alpha_\phi, \alpha_w, \alpha_\lambda]$ for rotation angles ϕ , observable weights w and scaling parameters λ , respectively. For softmax-VQCs, we take a linear annealing schedule for the inverse temperature parameter β starting from 1 and ending up in the final β . The batch size is counted in number of episodes used to evaluate the gradient of the value function. Depth indicates the number of encoding layers D_{enc} for VQC policies, or the number of hidden layers for a NN policy. Width corresponds to the number of qubits n on which acts a VQC (also equal to the dimension d of the environment's state space), or the number of units per hidden layer for a NN.

Each function $f_s : \mathbb{Z}_p^* \rightarrow \{-1, 1\}$ hence labels half the elements in \mathbb{Z}_p^* with a label +1 and the other half with a label -1. We refer to Figure 1 in Ref. [16] for a good visualization of all these objects here defined.

The performance of a classifier f is measured in terms of its testing accuracy

$$\text{Acc}_f(f_s) = \Pr_{x \sim \mathcal{X}}[f(x) = f_s(x)].$$

Appendix H: Proof of Theorem 2

In the following, we provide constructions of *a*) fully random, *b*) partially random and *c*) fully deterministic environments satisfying the properties of Theorem 2. We will consider the three families of environments separately and provide individual lemmas specifying their exact separation properties.

Environment	Model	Entang. topology	Train entang.	Observables	Number of params.	Baseline
CartPole-v1	softmax-VQC	All-to-all	Yes	$[wZ_0Z_1Z_2Z_3, (-\dots)]$	$\{24, 88\}$	No
	raw-VQC	All-to-all	Yes	$[Z_0Z_1Z_2Z_3, (-\dots)]$	$\{25, 89\}$	No
MountainCar-v0	softmax-VQC	One-to-one	No	$[w_0Z_0, w_1Z_0Z_1, w_2Z_1]$	$\{39, 55\}$	Yes
	raw-VQC	One-to-one	No	$[P_{0,1}, P_2, P_3]$	$\{36, 52\}$	Yes
Acrobot-v1	softmax-VQC	Circular	Yes	$[\mathbf{w}_i \cdot (Z_0, \dots, Z_5)^T]_{1 \leq i \leq 3}$	$\{66, 138\}$	Yes
	raw-VQC	Circular	Yes	$[P_{0..21}, P_{22..42}, P_{43..63}]$	$\{60, 132\}$	Yes
SL-VQC	softmax-VQC	One-to-one	No	$[wZ_0Z_1, (-\dots)]$	37	No
	DNN	\times	\times	\times	902	No
Cliffwalk-VQC	softmax-VQC	One-to-one	No	$[wZ_0Z_1, (-\dots)]$	37	No
	DNN	\times	\times	\times	902	No

Table III. **Hyperparameters 2/2.** Circular and all-to-all topologies of entangling layers are equivalent for $n = 2$ qubits, so we call them one-to-one in that case. When trained, entangling layers are composed of ZZ -rotations, otherwise, they are composed of CZ gates. For policies with 2 actions, the same observable, up to a sign change, is used for both actions. Z_i refers to a Pauli Z observable acting on qubit i , while $P_{i..j}$ indicates a projector on basis states i to j . In the experiments of Sec. V C, when the weights of the softmax-VQC are kept fixed, the observables used for MountainCar-v0 and Acrobot-v1 are $[Z_0, Z_0Z_1, Z_1]$, and those used for CartPole-v1 are $[Z_0Z_1Z_2Z_3, -Z_0Z_1Z_2Z_3]$. The different number of parameters in a given row correspond to the different depths in that same row in Table II.

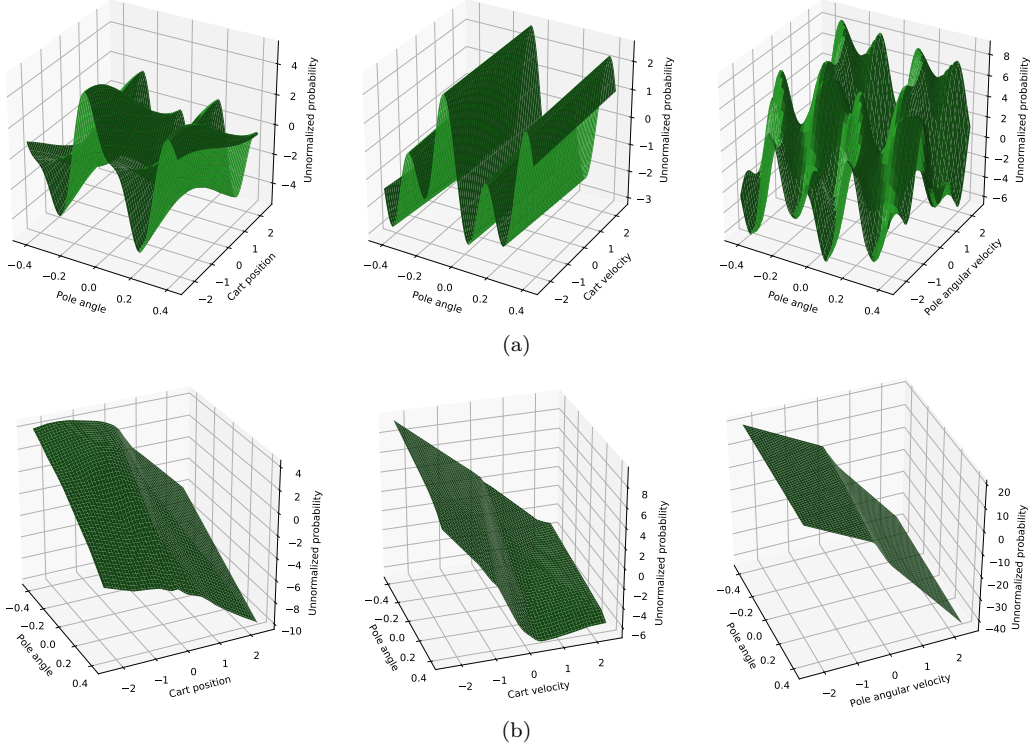


Figure 6. **Prototypical unnormalized policies learned by softmax-VQC agents and DNN agents in CartPole.** Due to the 4 dimensions of the state space in CartPole, we represent the unnormalized policies learned by (a) softmax-VQC agents and (b) DNN agents on 3 subspaces of the state space by fixing unrepresented dimensions to 0 in each plot. To get the probability of the agent pushing the cart to the left, one should apply the logistic function (i.e., 2-dimensional softmax) $1/(1 + \exp(-z))$ to the z -axis values of each plot.

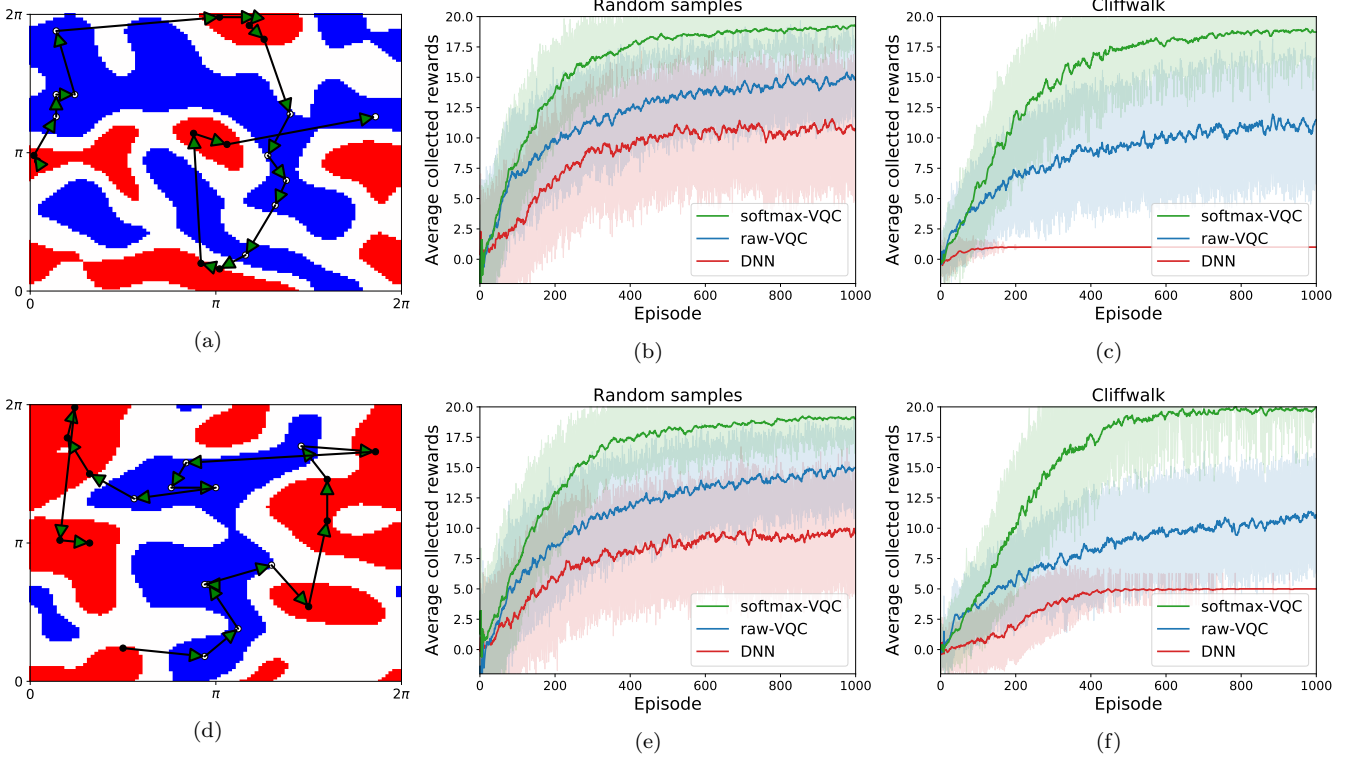


Figure 7. **Different random initializations of VQC-generated environments and their associated learning curves.** See Fig. 5 for details. The additional learning curves (20 agents per curve) of randomly-initialized raw-VQC agents highlight the hardness of these environments for VQC policies drawn from the same family as the environment-generating VQCs.

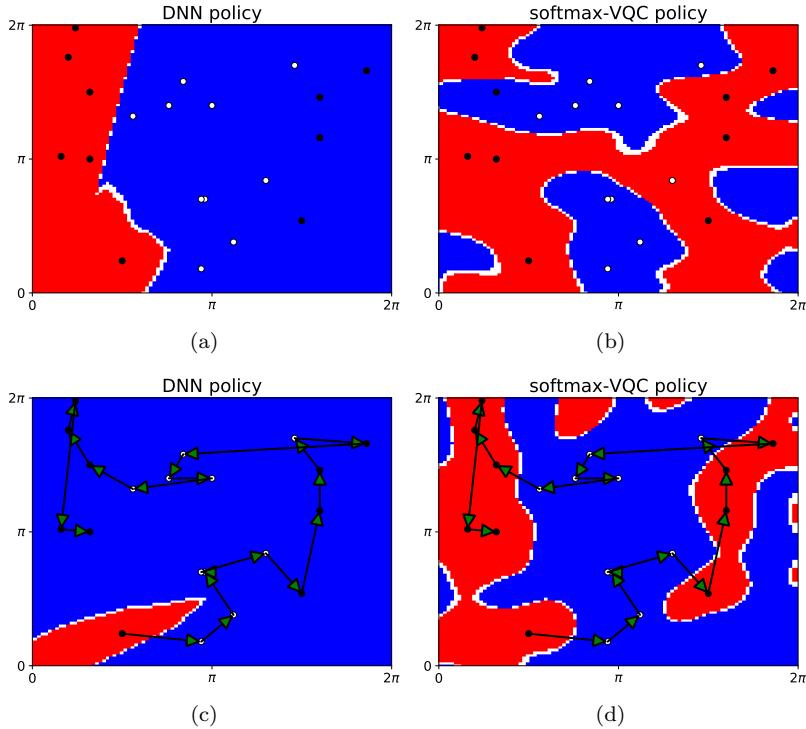


Figure 8. **Prototypical policies learned by softmax-VQC agents and DNN agents in VQC-generated environments.** All policies are associated to the labeling function of Fig. 7.d. Policies (a) and (b) are learned in the random-sampling environment while policies (c) and (d) are learned in the cliffwalk environment.

a. Fully random: the SL-DLP environment. This result is near-trivially obtained by noting that any classification problem can be easily mapped to a (degenerate) RL problem. For this, the environment will be an MDP defined as follows: its state space is the input space of the classification problem, its action space comprises all possible labels, rewards are trivially $+1$ for assigning a correct label to an input state and -1 otherwise, and the initial and next-state transition probabilities are state-independent and equal to the input distribution of the classification task. The optimal policy of this MDP is clearly the optimal classifier of the corresponding SL task. Consider now the classification task of Liu *et al.*, defined in detail in Appendix G: the input distribution is taken to be uniform on the state space, i.e., $P(s_t) = \frac{1}{|S|}$, and the performance of a classifier f w.r.t. a labeling (or ground truth) function f^* is measured in terms of a testing accuracy

$$\text{Acc}_f(f^*) = \frac{1}{|S|} \sum_s \mathbb{1}[f(s) = f^*(s)]. \quad (\text{H1})$$

For the MDP associated to this classification task and length-1 episodes of interaction, the value function of any policy $\pi(a|s)$ is given by

$$\begin{aligned} V_\pi(s_0) &= \frac{1}{|S|} \sum_{s_0} (\pi(f^*(s_0)|s_0) - \pi(-f^*(s_0)|s_0)) \\ &= \frac{1}{|S|} \sum_{s_0} 2\pi(f^*(s_0)|s_0) - 1 \\ &= 2\text{Acc}_\pi(f^*) - 1, \end{aligned}$$

which is trivially related to the testing accuracy of this policy on the classification task. Note that we also have $V_{\text{rand}}(s_0) = 0$ and $V_{\text{opt}}(s_0) = 1$.

Since these observations hold irrespectively of the labeling function f^* , we can show the following result:

Lemma 3 (Quantum advantage in SL-DLP). *There exists a uniform family of SL-DLP MDPs, each derived from a labeling function f^* of the DLP concept class \mathcal{C} (see Appendix G), for which classical hardness and quantum learnability holds. More specifically, the performance of any classical learner is upper bounded by $1/\text{poly}(n)$, while that of a class of quantum agents is lower bounded by 0.98 with probability above $2/3$ (over the randomness of their interaction with the environment and noise in their implementation).*

Proof. Classical hardness is trivially obtained by contraposition: assuming no classical polynomial-time algorithm can solve DLP, then using Theorem 1 of Liu *et al.*, any classical policy would have testing accuracy $\text{Acc}_\pi(f^*) \leq 1/2 + 1/\text{poly}(n)$, and hence its value function would be $V_\pi(s_0) \leq 1/\text{poly}(n)$.

For quantum learnability, we define an agent that first collects $\text{poly}(n)$ random length-1 interactions (i.e., a random state s_0 and its associated reward for an action $+1$,

from which the label $f^*(s_0)$ can be inferred), and use Theorem 2 of Liu *et al.* to train a classifier that has test accuracy at least 0.99 with probability at least $2/3$ (this process can be repeated $\mathcal{O}(\log(\delta^{-1}))$ times to increase this probability to $1 - \delta$ via majority voting). This classifier has a value function $V_\pi(s_0) \geq 0.98$. \square

Note that this proof trivially generalizes to episodes of interaction with length greater than 1, when preserving the absence of temporal correlation in the states experienced by the agents. For episodes of length H , the only change is that the value function of any policy, and hence the bounds we achieve, get multiplied by a factor of $\frac{1-\gamma^H}{1-\gamma}$ for a discount factor $\gamma < 1$ and by a factor H for $\gamma = 1$.

b. Partially random: the Cliffwalk-DLP environment. One major criticism to the result of Lemma 3 is that it applies to a very degenerate, fully random RL environment. In the following, we show that similar results can be obtained in environments based on the same classification problem, but while imposing more temporal structure and less randomness (such constructions were introduced in Ref. [29], but for the purpose of query separations between RL and QRL). For instance, one can consider cliffwalk-type environments, inspired by the textbook “cliff walking” environment of Sutton & Barto [25]. This class of environments differs from the previous SL-DLP environments in its state and reward structure: in any episode of interaction, experienced states follow a fixed “path” structure (that of the cliff) for correct actions, and a wrong action yields to immediate “death” (negative reward and episode termination). We slightly modify this environment to a “slippery scenario” in which, with a δ probability, any action may lead to a uniformly random position on the cliff. This additional randomness allows us to prove the following separation:

Lemma 4 (Quantum advantage in Cliffwalk-DLP). *There exists a uniform family of Cliffwalk-DLP MDPs with arbitrary slipping probability $\delta \in [0.86, 1]$ and discount factor $\gamma \in [0, 0.9]$, each derived from a labeling function f^* of the DLP concept class \mathcal{C} , for which classical hardness and quantum learnability holds. More specifically, the performance of any classical learner is upper bounded by $V_{\text{rand}}(s_0) + 0.1$, while that of a class of quantum agents is lower bounded by $V_{\text{opt}}(s_0) - 0.1$ with probability above $2/3$ (over the randomness of their interaction with the environment and noise in their implementation). Since $V_{\text{rand}}(s_0) \leq -\frac{1}{2}$ and $V_{\text{opt}} = 0$, we always have a classical-quantum separation.*

The proof of this lemma is deferred to Appendix I for clarity.

c. Fully deterministic: the Deterministic-DLP environment. The simplest example of a deterministic RL environment where separation can be proven is a partially observable MDP (POMDP) defined as follows: it

constitutes a 1-D chain of states of length $k + 2$, where k is $\text{poly}(n)$. We refer to the first k states as “training states”, and we call the last two states “test” and “limbo” states, respectively. The training states are of the form $(x, f_s(x))$, i.e., a point uniformly sampled and its label. The actions are $+1, -1$, and both lead to the same subsequent state on the chain (since the same $(x, f_s(x))$ can appear twice in the chain, this is the reason why the environment is partially observable), and no reward is given for the first k states. In the test state, the agent is only given a point x with no label. A correct action provides a reward of 1 and leads to the beginning of the chain, while an incorrect action leads to the limbo state, which self-loops for both actions and has no rewards. In other words, after poly-many examples where the agent can learn the correct labeling, it is tested on one state. Failure means it will never obtain a reward.

For each concept f_s , we define exponentially many environments obtained by random choices of the states appearing in the chain. In a given instance, call $T = (x_0, \dots, x_{k-1})$ the training states of that instance, x_k its testing state and l its limbo state. The interaction of an agent with the environment is divided into episodes of length $k + 1$, but the environment keeps memory of its state between episodes. This means that, while the first episode starts in x_0 , depending on the performance of the agent, later episodes start either in x_0 or in l . For a policy π , we define the value $V_\pi(s_0)$ as the expected reward⁶ of this policy in any episode of length $k + 1$ with an initial state $s_0 \in \{x_0, l\}$. Since the testing state x_k is the only state to be rewarded, we can already note that $V_\pi(x_0) = \pi(f^*(x_k)|T, x_k)$, that is, the probability of the policy correctly labeling the testing state x_k after having experienced the training states T . Also, since $s_0 \in \{x_0, l\}$ and $V_\pi(l) = 0$, we have $V_\pi(x_0) \geq V_\pi(s_0)$.

With this construction, we obtain the following result:

Lemma 5 (Quantum advantage in Deterministic-DLP). *There exists a uniform family of Deterministic-DLP POMDPs (exponentially many instances for a given concept f_s of the DLP classification problem) where:*

1) (classical hardness) *if there exists a classical learning agent which, when placed in a randomly chosen instance of the environment, has value $V_c(s_0) \geq 1/2 + 1/\text{poly}(n)$ (that is, $1/\text{poly}(n)$ better than a random agent), with probability at least 0.845 over the choice of environment and the randomness of its learning algorithm, then there exists an efficient classical algorithm to solve DLP, and,*

2) (quantum learnability) *there exists a class of quantum agents that attains a value $V_q(s_0) = 1$ (that is, the optimal value) with probability at least 0.98 over the choice of environment and randomness of the learning algorithm.*

The proof of this lemma is deferred to Appendix J for clarity.

⁶ Note that we assume here a discount factor $\gamma = 1$, but our results would also hold for an arbitrary $\gamma > 0$, if we scale the reward of the testing state to γ^{-k} .

By combining our three lemmas, and taking the weakest separation claim for the cases *ii*) and *iii*), we get Theorem 2. For the interested reader, we list the following remarks, relating to the proofs of these lemmas:

- SL-DLP and Deterministic-DLP are the two closest environments to the DLP classification task of Liu *et al.* While the value function in SL-DLP is trivially equivalent to the accuracy of the classification problem, we find the value function in Deterministic-DLP to be *weaker* than this accuracy. Namely, a high accuracy trivially leads to a high value while a high (or non-trivial) value doesn’t necessarily lead to a high (or non-trivial) accuracy (in all these cases, the high probability over the randomness of choosing the environments and of the learning algorithms is implied). This explains why the classical hardness statement for Deterministic-DLP is weaker than in SL-DLP.
- In Cliffwalk-DLP, it is less straightforward to relate the testing accuracy of a policy to its performance on the deterministic parts of the environment, which explains why we trivially upper bound this performance by 0 on these parts. We believe however that these deterministic parts will actually make the learning task much harder, since they strongly restrict what part of the state space the agents can see. This claim is supported by our numerical experiments in Sec. VI B. Also, since we showed classical hardness for fully deterministic environments, it would be simple to construct a variant of Cliffwalk-DLP where these deterministic parts would be provably classically hard as well.

Appendix I: Proof of Lemma 4

Consider a slippery cliffwalk environment defined by a labeling function f^* in the concept class \mathcal{C} of Liu *et al.* This cliffwalk has $p - 1$ states ordered, w.l.o.g., in their natural order, and correct actions (the ones that do not lead to immediate “death”) $f^*(i)$ for each state $i \in \mathbb{Z}_p^*$. For simplicity of our proofs, we also consider circular boundary conditions (i.e, doing the correct action on the state $p - 1$ of the cliff leads to the state 1), random slipping at each interaction step to a uniformly sampled state on the cliff with probability $\delta > 0$, an initialization of each episode in a uniformly sampled state $i \in \mathbb{Z}_p^*$, and a 0 (-1) reward for doing the correct (wrong) action in any given state.

1. Upper bound on the value function

The value function of any policy π which has probability $\pi(i)$ (we abbreviate $\pi(f^*(i)|i)$ to $\pi(i)$) of doing the correct action in state $i \in \mathbb{Z}_p^*$ is given by:

$$V_\pi(i) = \pi(i)\gamma \left((1-\delta)V_\pi(i+1) + \delta \frac{1}{p-1} \sum_{j=1}^{p-1} V_\pi(j) \right) - (1-\pi(i)) \quad (\text{I1})$$

Since this environment only has negative rewards, we have that $V_\pi(i) \leq 0$ for any state i and policy π , which allows us to write the following inequality:

$$V_\pi(i) \leq \pi(i)\gamma \left(\delta \frac{1}{p-1} \sum_{j=1}^{p-1} V_\pi(j) \right) - (1-\pi(i))$$

We use this inequality to bound the following term:

$$\begin{aligned} & \frac{1}{p-1} \sum_{i=1}^{p-1} V_\pi(i) \\ & \leq \frac{1}{p-1} \sum_{i=1}^{p-1} \left(\pi(i) \frac{\gamma\delta}{p-1} \sum_{j=1}^{p-1} V_\pi(j) - (1-\pi(i)) \right) \\ & = \left(\frac{1}{p-1} \sum_{i=1}^{p-1} \pi(i) \right) \left(\frac{\gamma\delta}{p-1} \sum_{j=1}^{p-1} V_\pi(j) + 1 \right) - 1 \end{aligned}$$

We note that the first factor is exactly the accuracy of the policy π on the classification task of Liu *et al.*:

$$\text{Acc}_\pi(f^*) = \frac{1}{p-1} \sum_{i=1}^{p-1} \pi(i).$$

We hence have:

$$\frac{1}{p-1} \sum_{i=1}^{p-1} V_\pi(i) \leq \text{Acc}_\pi(f^*) \left(\gamma \delta \frac{1}{p-1} \sum_{j=1}^{p-1} V_\pi(j) + 1 \right) - 1$$

which is equivalent to:

$$\frac{1}{p-1} \sum_{i=1}^{p-1} V_\pi(i) \leq \frac{\text{Acc}_\pi(f^*) - 1}{1 - \text{Acc}_\pi(f^*)\gamma\delta}$$

when $\text{Acc}_\pi(f^*)\gamma\delta < 1$.

We now note that this average value function is exactly the value function evaluated on the initial state s_0 of the agent, since this state is uniformly sampled from \mathbb{Z}_p^* for every episode. Hence,

$$V_\pi(s_0) \leq \frac{\text{Acc}_\pi(f^*) - 1}{1 - \text{Acc}_\pi(f^*)\gamma\delta} \quad (\text{I2})$$

2. Lower bound on the value function

Again, by noting in Eq. (I1) that we have $V_\pi(i) \leq 0$ and $\pi(i) \leq 1$ for any policy π and state $i \in \mathbb{Z}_p^*$, we have:

$$V_\pi(i) \geq \gamma \left((1-\delta)V_\pi(i+1) + \delta \frac{1}{p-1} \sum_{j=1}^{p-1} V_\pi(j) \right) - (1-\pi(i))$$

We use this inequality to bound the value function at the initial state s_0 :

$$\begin{aligned} V_\pi(s_0) &= \frac{1}{p-1} \sum_{i=1}^{p-1} V_\pi(i) \\ &\geq \gamma \left(\frac{1-\delta}{p-1} \sum_{i=1}^{p-1} V_\pi(i+1) + \frac{\delta}{p-1} \sum_{j=1}^{p-1} V_\pi(j) \right) \\ &\quad + \frac{1}{p-1} \sum_{i=1}^{p-1} \pi(i) - 1 \\ &= \gamma ((1-\delta)V_\pi(s_0) + \delta V_\pi(s_0)) + \text{Acc}_\pi(f^*) - 1 \\ &= \gamma V_\pi(s_0) + \text{Acc}_\pi(f^*) - 1 \end{aligned}$$

by using the circular boundary conditions of the cliffwalk in the third line.

This inequality is equivalent to:

$$V_\pi(s_0) \geq \frac{\text{Acc}_\pi(f^*) - 1}{1 - \gamma} \quad (\text{I3})$$

when $\gamma < 1$.

3. Bounds for classical hardness and quantum learnability

We use the bounds derived in the two previous sections to prove classical hardness and quantum learnability of this task environment, as stated in Lemma 4.

For this, we start by noting the following expression for the value function of a random policy (one that does random actions in all states):

$$\begin{aligned} V_{\text{rand}}(s_0) &= \frac{\gamma}{2} \left(\frac{1-\delta}{p-1} \sum_{i=1}^{p-1} V_{\text{rand}}(i+1) + \frac{\delta}{p-1} \sum_{j=1}^{p-1} V_{\text{rand}}(j) \right) - \frac{1}{2} \\ &= \frac{\gamma}{2} V_{\text{rand}}(s_0) - \frac{1}{2} = -\frac{1}{2-\gamma} \end{aligned}$$

again due to the circular boundary conditions of the cliffwalk and the resulting absence of termination conditions outside of “death”.

As for the value function of the optimal policy, this is trivially $V_{\text{opt}} = 0$.

a. Proof of classical hardness

For any policy π , we define the function $g(x, \delta, \gamma) = V(x, \delta, \gamma) - V_{\text{rand}}(\gamma)$, where we adopt the short-hand notation $x = \text{Acc}_\pi(f^*)$ and call V the upper bound on the value function $V_\pi(s_0)$ of π . The expression of $g(x, \delta, \gamma)$ (for $(x, \delta, \gamma) \neq (1, 1, 1)$) is given by:

$$g(x, \delta, \gamma) = \frac{x-1}{1-\delta\gamma x} + \frac{1}{2-\gamma} \quad (\text{I4})$$

To prove classical hardness, it is sufficient to show that $x \leq 0.51$ implies $g(x, \delta, \gamma) \leq 0.1$ for $\delta \in [\delta_0, 1]$, $\gamma \in [0, \gamma_1]$ and a $\{\delta_0, \gamma_1\}$ pair of our choosing. To see this, notice that the contraposition gives $x = \text{Acc}_\pi(f^*) > 0.51$ which is sufficient to construct an efficient algorithm that solves DLP. To achieve this result, we show the three following inequalities, $\forall x \leq 0.51$ and $\forall (\delta, \gamma) \in [\delta_0, 1] \times [0, \gamma_1]$:

$$g(x, \delta, \gamma) \stackrel{(i)}{\leq} g(0.51, \delta, \gamma) \stackrel{(ii)}{\leq} g(0.51, \delta_0, \gamma) \stackrel{(iii)}{\leq} g(0.51, \delta_0, \gamma_1)$$

where δ_0 and γ_1 are chosen such that $g(0.51, \delta_0, \gamma_1) \leq 0.1$.

Proof of (i). We look at the derivative of g w.r.t. x :

$$\frac{\partial g(x, \delta, \gamma)}{\partial x} = \frac{1 - \delta\gamma}{(1 - \delta\gamma x)^2} \geq 0 \quad \forall (x, \delta, \gamma) \in [0, 1]^3 \setminus (1, 1, 1)$$

and hence g is an increasing function of x , which gives our inequality. \square

Proof of (ii). We look at the derivative of g w.r.t. δ :

$$\frac{\partial g(x, \delta, \gamma)}{\partial \delta} = \frac{\gamma(x-1)x}{(1 - \delta\gamma x)^2} \leq 0 \quad \forall (x, \delta, \gamma) \in [0, 1]^3 \setminus (1, 1, 1)$$

and hence g is a decreasing function of δ , which gives our inequality. \square

Proof of (iii). We look at the derivative of g w.r.t. γ :

$$\frac{\partial g(x, \delta, \gamma)}{\partial \gamma} = \frac{\delta(x-1)x}{(1 - \delta\gamma x)^2} + \frac{1}{(2 - \gamma)^2} \quad \forall (x, \delta, \gamma) \in [0, 1]^3 \setminus (1, 1, 1)$$

We have:

$$\frac{\partial g(x, \delta, \gamma)}{\partial \gamma} \geq 0 \Leftrightarrow ((\delta x)^2 + \delta(x^2 - x)) \gamma^2 - 2\delta(2x^2 - x)\gamma + 4\delta(x^2 - x) + 1 \geq 0$$

By setting $x = 0.51$ and $\delta = 0.86$, we find

$$\frac{\partial g(0.51, 0.86, \gamma)}{\partial \gamma} \geq 0 \quad \forall \gamma \in [0, 1]$$

since the roots of the second-degree polynomial above are approximately $\{-2.91, 2.14\}$ and we have $(\delta x)^2 + \delta(x-1)x \approx -0.0225 < 0$.

Hence $g(0.51, \delta_0, \gamma)$ is an increasing function of γ , which gives our inequality. \square

Given that $g(0.51, 0.86, 0.9) \approx 0.0995 < 0.1$, we then get our desired result for $\delta_0 = 0.86$ and $\gamma_1 = 0.9$. Noting that $V_\pi(s_0) - V_{\text{rand}}(\gamma) \leq g(x, \delta, \gamma) \leq 0.1$ from Eq. (I2), we hence have classical hardness $\forall (\delta, \gamma) \in [\delta_0, 1] \times [0, \gamma_1]$.

b. Proof of quantum learnability

Proving quantum learnability is more trivial, since, for $\text{Acc}_\pi(f^*) \geq 0.99$ and $\gamma \leq 0.9$, we directly have, using Eq. (I3):

$$V_\pi(s_0) \geq -0.1 = V_{\text{opt}} - 0.1$$

To conclude this proof, we still need to show that we can obtain in this environment a policy π such that $\text{Acc}_\pi(f^*) \geq 0.99$ with high probability. For that, we use agents that first collect $\text{poly}(n)$ *distinct* samples (states s and their inferred labels $f^*(s)$) from the environment (distinct in order to avoid biasing the distribution of the dataset with the cliffwalk temporal structure). This can be done efficiently in $\text{poly}(n)$ interactions with the environment, since each episode is initialized in a random state $s_0 \in \mathbb{Z}_p^*$. We then use the learning algorithm of Liu *et al.* to train a classifier π with the desired accuracy, with high probability.

Appendix J: Proof of Lemma 5

1. Proof of classical hardness

Suppose that a polynomial-time classical agent achieves a value $V_c(s_0) \geq \frac{1}{2} + \frac{1}{\text{poly}(n)}$ with probability $(1 - \delta)$ over the choice of environment and the randomness of its learning algorithm. We call “success” the event $V_c(s_0) \geq \frac{1}{2} + \frac{1}{\text{poly}(n)}$ and S_δ the subset of the instances $S = \{T, x_k\}$ for which, theoretically, a run of the agent would “succeed” (this is hence a set that depends on the randomness of the agent).

Note that, on every instance in S_δ , $\pi(f^*(x_k)|T, x_k) = V_c(x_0) \geq V_c(s_0) \geq \frac{1}{2} + \frac{1}{\text{poly}(n)}$. Since this probability is bounded away from $1/2$ by an inverse polynomial, this means that we can “boost” it to a larger probability $(1 - \varepsilon)$. More specifically, out of the policy π obtained after interacting for k steps with the environment, we define a classifier f_c acting on x_k such that we sample $\mathcal{O}(\log(\varepsilon^{-1}))$ -many times from $\pi(a|T, x_k)$ and label x_k by majority vote. For the instances in S_δ , the probability of correctly labeling x_k is $\Pr[f_c(x_k) = f^*(x_k)] \geq 1 - \varepsilon$.

Define $P(T) = \Pr[T = T]$ and $P(x_k) = \Pr[x_k = x_k]$ the probabilities of sampling certain training states T and a testing state x_k , when choosing an instance of the environment. We now look at the following quantity:

$$\begin{aligned} & \mathbb{E}_{P(T)} [\text{Acc}_{f_c}(T)] \\ &= \sum_T P(T) \sum_{x_k} P(x_k) \Pr[f_c(x_k) = f^*(x_k)|T, x_k] \\ &= \sum_{T, x_k} P(T, x_k) \Pr[f_c(x_k) = f^*(x_k)|T, x_k] \end{aligned}$$

$$\begin{aligned}
&\geq \sum_{T,x_k} P(T, x_k) \Pr[\text{success}|T, x_k] \\
&\quad \times \Pr[f_c(x_k) = f^*(x_k)|T, x_k, \text{success}] \\
&\geq (1 - \delta)(1 - \varepsilon)
\end{aligned}$$

since $\Pr[f_c(x_k) = f^*(x_k)|T, x_k] \geq 1 - \varepsilon$ for instances in S_δ and $\sum_{T,x_k} P(T, x_k) \Pr[\text{success}|T, x_k] \geq 1 - \delta$ by definition.

In the following, we set $1 - \varepsilon = 0.999$ and $1 - \delta \geq 0.845$ (the reason for this becomes apparent below), such that:

$$\mathbb{E}_{P(T)} [\text{Acc}_{f_c}(T)] \geq 0.844155 > \frac{5}{6} + \frac{1}{96} \quad (\text{J1})$$

Now, consider the following learning algorithm: given a training set T , construct a Deterministic-DLP environment that uses this T and a randomly chosen x_k , and define the classifier f_c that boosts the $\pi(a|T, x_k)$ obtained by running our classical agent on this environment (as explained above). We want to show that f_c has accuracy $\text{Acc}_{f_c}(T) \geq \frac{1}{2} + \frac{1}{\text{poly}(n)}$ with probability at least $2/3$ over the choice of T and the randomness of its construction, which is sufficient to solve DLP classically. For that, we show a stronger statement. Call $\mathcal{T}_{\text{succ}}$ the subset of all instances of training states $\mathcal{T} = \{T\}$ for which $\text{Acc}_{f_c}(T) \geq \frac{1}{2} + \frac{1}{\text{poly}(n)}$. We prove by contradiction that $|\mathcal{T}_{\text{succ}}| \geq \frac{2|\mathcal{T}|}{3}$:

Assume $|\mathcal{T}_{\text{succ}}| < \frac{2|\mathcal{T}|}{3}$, then

$$\begin{aligned}
\mathbb{E}_{P(T)} [\text{Acc}_{f_c}(T)] &= \sum_T P(T) \text{Acc}_{f_c}(T) \\
&= \frac{1}{|\mathcal{T}|} \left(\sum_{T \in \mathcal{T}_{\text{succ}}} \text{Acc}_{f_c}(T) + \sum_{T \notin \mathcal{T}_{\text{succ}}} \text{Acc}_{f_c}(T) \right) \\
&< \frac{|\mathcal{T}_{\text{succ}}|}{|\mathcal{T}|} \times 1 + \frac{|\mathcal{T}| - |\mathcal{T}_{\text{succ}}|}{|\mathcal{T}|} \left(\frac{1}{2} + \frac{1}{\text{poly}(n)} \right) \\
&< \frac{5}{6} + \frac{1}{3\text{poly}(n)} < 0.844155
\end{aligned}$$

for large enough n , in contradiction with Eq. (J1).

Hence, with probability at least $2/3$ over the choice of training states and the randomness of the learning algorithm, our constructed classifier has accuracy $\text{Acc}_{f_c}(T) \geq \frac{1}{2} + \frac{1}{\text{poly}(n)}$. By using Theorem 8, Remark 1 of Liu *et al.*, this is sufficient to construct an efficient classical algorithm that solves DLP.

2. Proof of quantum learnability

Using the learning algorithm of Liu *et al.*, we can construct a quantum classifier that achieves accuracy $\text{Acc}_q(T) \geq 0.99$ with probability at least $2/3$ over the randomness of the learning algorithm and the choice of training states T , of length $|T| = \text{poly}(n)$. Now define

instead training states T of length $|T| = M\text{poly}(n)$, for $M = \mathcal{O}(\log(\delta'^{-1}))$ (hence $|T|$ is still polynomial in n), and use each of the M segments of T to train M independent quantum classifiers. Define f_q as a classifier that labels x_k using a majority vote on the labels assigned by each of these classifiers. This constructed classifier has accuracy $\text{Acc}_{f_q}(T) \geq 0.99$ with now probability $1 - \delta'$ over the choice of training states T and the randomness of the learning algorithm.

We then note that, by calling “success” the event $\text{Acc}_{f_q}(T) \geq 0.99$, we have:

$$\begin{aligned}
&\sum_{T,x_k} P(T, x_k) \Pr[V_q(x_0) = 1|T, x_k] \\
&\geq \sum_T P(T) \sum_{x_k} P(x_k) \Pr[\text{success}|T] \\
&\quad \times \Pr[V_q(x_0) = 1|T, x_k, \text{success}] \\
&= \sum_T P(T) \Pr[\text{success}|T] \sum_{x_k} P(x_k) \\
&\quad \times \Pr[f_q(x_k) = f^*(x_k)|T, x_k, \text{success}] \\
&= \sum_T P(T) \Pr[\text{success}|T] \text{Acc}_{f_q}(T) \\
&\geq (1 - \delta') \times 0.99
\end{aligned}$$

which means that our constructed agent achieves a value $V_q(x_0) = 1$ (which also implies $V_q(s_0) = 1$) with probability at least $(1 - \delta') \times 0.99$ over the choice of environment and the randomness of the learning algorithm. By setting $(1 - \delta') = 0.98/0.99$, we get our statement.

Appendix K: Construction of a VQC agent for the DLP environments

In the two following Appendices, we construct a VQC classifier that can achieve close-to-optimal accuracy on the classification task of Liu *et al.* [16] (see Appendix G), and can hence also be used as a learning model in the DLP environments defined in Sec. VIA.

1. Description of the VQC classifier

As described in Sec. VIA, our classifier belongs to a family of so-called explicit quantum SVMs. It is hence described by a VQC with two parts: a feature-encoding unitary $U(x)$, which creates features $|\phi(x)\rangle = U(x)|0^{\otimes n}\rangle$ when applied to an all-0 state, followed by a variational circuit $V(\boldsymbol{\theta})$ parametrized by a vector $\boldsymbol{\theta}$. The resulting quantum state is then used to measure the expectation value $\langle O \rangle_{x,\boldsymbol{\theta}}$ of an observable O , to be defined. We rely on the same feature-encoding unitary $U(x)$ as the one used by Liu *et al.*, i.e., the unitary that creates feature

states of the form

$$|\phi(x)\rangle = \frac{1}{\sqrt{2^k}} \sum_{i=0}^{2^k-1} |x \cdot g^i\rangle \quad (\text{K1})$$

for $k = n - t \log(n)$, where t is a constant defined later, under noise considerations. This feature state can be seen as the uniform superposition of the image (under exponentiation $s' \mapsto g^{s'}$) of an interval of integers $[\log_g(x), \log_g(x) + 2^k - 1]$ in log-space. Note that $U(x)$ can be implemented in $\tilde{\mathcal{O}}(n^3)$ operations [16].

By noting that every labeling functions $f_s \in \mathcal{C}$ to be learned (see Eq. (G1)) is delimiting two equally-sized intervals of $\log(\mathbb{Z}_p^*)$, we can restrict the decision boundaries to be learned by our classifier to be half-space dividing hyperplanes in log-space. In feature space, this is equivalent to learning separating hyperplanes that are normal to quantum states of the form:

$$|\phi_{s'}\rangle = \frac{1}{\sqrt{(p-1)/2}} \sum_{i=0}^{(p-3)/2} |g^{s'+i}\rangle. \quad (\text{K2})$$

Noticeably, for input points x such that $\log_g(x)$ is away from some delimiting regions around s and $s + \frac{p-3}{2}$, we can notice that the inner product $|\langle\phi(x)|\phi_s\rangle|^2$ is either $\Delta = \frac{2^{k+1}}{p-1}$ or 0, whenever x is labeled +1 or -1 by f_s , respectively. This hence leads to a natural classifier to be built, assuming overlaps of the form $|\langle\phi(x)|\phi_{s'}\rangle|^2$ can be measured:

$$h_{s'}(x) = \begin{cases} 1, & \text{if } |\langle\phi(x)|\phi_{s'}\rangle|^2/\Delta \geq 1/2, \\ -1, & \text{otherwise} \end{cases} \quad (\text{K3})$$

which has an (ideal) accuracy $1 - \Delta$ whenever $s' = s$.

To complete the construction of our VQC classifier, we should hence design the composition of its variational part $V(\boldsymbol{\theta})$ and measurement O such that they result in expectation values of the form $\langle O \rangle_{x, \boldsymbol{\theta}} = |\langle\phi(x)|\phi_{s'}\rangle|^2$. To do this, we note that, for $|\phi_{s'}\rangle = \hat{V}(s')|0\rangle$, the following equality holds:

$$\begin{aligned} |\langle\phi(x)|\phi_{s'}\rangle|^2 &= \left| \langle 0^{\otimes n} | \hat{V}(s')^\dagger U(x_i) | 0^{\otimes n} \rangle \right|^2 \\ &= \text{Tr} [|0^{\otimes n}\rangle \langle 0^{\otimes n}| \rho(x, s')] \end{aligned}$$

where $\rho(x, s') = |\psi(x, s')\rangle \langle \psi(x, s')|$ is the density matrix of the quantum state $|\psi(x, s')\rangle = \hat{V}(s')^\dagger U(x_i) |0^{\otimes n}\rangle$. Hence, an obvious choice of variational circuit is $V(\boldsymbol{\theta}) = \hat{V}(s')$, combined with a measurement operator $O = |0^{\otimes n}\rangle \langle 0^{\otimes n}|$. Due to the similar nature of $|\phi_s'\rangle$ and $|\phi(x)\rangle$, it is possible to use an implementation for $\hat{V}(s')$ that is similar to that of $U(x_i)$ (take $x_i = g^{s'}$ and $k \approx n/2$)⁷. We

also note that, for points x such that $\log_g(x)$ is $(p-1)\Delta/2$ away from the boundary regions of $h_{s'}$, the non-zero inner products $|\langle\phi(x)|\phi_{s'}\rangle|^2$ are equal to $\Delta = \mathcal{O}(n^{-t})$. These can hence be estimated efficiently to additive error, which allows for an efficient implementation of our classifier $h_{s'}$ (see Eq. (K3)).

2. Noisy classifier

In practice, there will be noise associated with the estimation of the inner products $|\langle\phi(x)|\phi_{s'}\rangle|^2$, namely due to the additive errors associated to sampling. Similarly to Liu *et al.*, we model noise by introducing a random variable $e_{is'}$ for each data point x_i and variational parameter $g^{s'}$, such that the estimated inner product is $|\langle\phi(x_i)|\phi_{s'}\rangle|^2 + e_{is'}$. This random variable satisfies the following equations:

$$\begin{cases} e_{is'} \in [-\Delta, \Delta] \\ \mathbb{E}[e_{is'}] = 0 \\ \text{Var}[e_{is'}] \leq 1/R \end{cases}$$

where R is the number of circuit evaluations used to estimate the inner product. We hence end up with a noisy classifier:

$$\tilde{h}_{s'}(x_i) = \begin{cases} 1, & \text{if } (|\langle\phi(x_i)|\phi_{s'}\rangle|^2 + e_{is'}) / \Delta \geq 1/2, \\ -1, & \text{otherwise} \end{cases}$$

The noise has the effect that some points which would be correctly classified by the noiseless classifier have now a non zero probability of being misclassified. To limit the overall decrease in classification accuracy, we focus on limiting the probability of misclassifying points x_i such that $\log_g(x_i)$ is $(p-1)\Delta/2$ away from the boundary points s' and $s' + \frac{p-3}{2}$ of $g_{s'}$. We call $I_{s'}$ the subset of \mathbb{Z}_p^* comprised of these points. For points in $I_{s'}$, the probability of misclassification is that of having $|e_{is'}| \geq \Delta/2$. We can use Chebyshev's inequality to bound this probability:

$$\Pr \left(|e_{is'}| \geq \frac{\Delta}{2} \right) \leq \frac{4}{\Delta^2 R} \quad (\text{K4})$$

since $\mathbb{E}[e_{is'}] = 0$ and $\text{Var}[e_{is'}] \leq 1/R$.

Appendix L: Proof of trainability of our VQC agent in the SL-DLP environment

In this Appendix, we describe an optimization algorithm to train the variational parameter $g^{s'}$ of the VQC classifier we defined in Appendix K. This task is non-trivial for three reasons: 1) even by restricting the separating hyperplanes accessible by our classifier, there are still $p - 1$ candidates, which makes an exhaustive search for the optimal one intractable; 2) noise in the evaluation of the classifier can potentially heavily perturb its

⁷ Note that we write $\hat{V}(s')$ and $U_{s'}$ to be parametrized by s' but the true variational parameter here is $g^{s'}$, since we work in input space and not in log-space.

loss landscape, which can shift its global minimum and 3) decrease the testing accuracy of the noisy classifier. Nonetheless, we show that all these considerations can be taken into account for a simple optimization algorithm, such that it returns a classifier with close-to-optimal accuracy with high probability of success. More precisely, we show the following Theorem:

Theorem 3. *For a training set of size n^c such that $c \geq \max\{\log_n(8/\delta), \log_n\left(\frac{\log(\delta/2)}{\log(1-2n^{-t})}\right)\}$ for $t \geq \max\{3\log_n(8/\delta), \log_n(16/\varepsilon)\}$ in the definition of Δ , and a number of circuit evaluations per inner product $R \geq \left\{\frac{4n^{2(t+c)}}{\delta}, \frac{128}{\varepsilon^3}\right\}$, then our optimization algorithm returns a noisy classifier $\tilde{h}_{s'}$ with testing accuracy $\text{Acc}_{\tilde{h}_{s'}}(f_s)$ on the DLP classification task of Liu et al. such that*

$$\Pr\left(\text{Acc}_{\tilde{h}_{s'}}(f_s) \geq 1 - \varepsilon\right) \geq 1 - \delta$$

The proof of this Theorem is detailed below.

Given a training set $X \subset \mathcal{X}$ polynomially large in n , i.e., $|X| = n^c$, define the training loss:

$$\mathcal{L}(s') = \frac{1}{2|X|} \sum_{x \in X} |h_{s'}(x) - f_s(x)|$$

and its noisy analog:

$$\tilde{\mathcal{L}}(s') = \frac{1}{2|X|} \sum_{x \in X} |\tilde{h}_{s'}(x) - f_s(x)|$$

Our optimization algorithm goes as follows: using the noisy classifier $\tilde{h}_{s'}$, evaluate the loss function $\tilde{\mathcal{L}}(\log_g(x))$ for each variational parameter $g^{s'} = x \in X$, then set

$$g^{s'} = \operatorname{argmin}_{x \in X} \tilde{\mathcal{L}}(\log_g(x)).$$

This algorithm is efficient in the size of the training set $|X|$, since it only requires $|X|^2$ evaluations of $\tilde{h}_{s'}$.

To prove Theorem 3, we show, first, that we can enforce $\operatorname{argmin}_{x \in X} \tilde{\mathcal{L}}(\log_g(x)) = \operatorname{argmin}_{x \in X} \mathcal{L}(\log_g(x))$ with high probability (Lemma 6), and second, that this algorithm also leads to s' close to the optimal s in log-space with high probability (Lemma 7).

Lemma 6. *For a training set of size n^c such that $c \geq \log_n(8/\delta)$, a $t \geq 3c$ in the definition of Δ , and a number of circuit evaluations per inner product $R \geq \frac{4n^{2(t+c)}}{\delta}$, we have*

$$\Pr\left(\operatorname{argmin}_{x \in X} \tilde{\mathcal{L}}(\log_g(x)) = \operatorname{argmin}_{x \in X} \mathcal{L}(\log_g(x))\right) \geq 1 - \frac{\delta}{2}$$

Proof. In order for the minima of the two losses to be obtained for the same $x \in X$, it is sufficient to ensure that the classifiers $h_{\log_g(x_i)}$ and $\tilde{h}_{\log_g(x_i)}$ agree on all points x_j , for all $(x_i, x_j) \in X$. This can be enforced by having:

$$\left(\bigcap_{\substack{i,j \\ i \neq j}} x_i \in I_{\log_g(x_j)}\right) \cap \left(\bigcap_{i,s'} |e_{i,s'}| \leq \frac{\Delta}{2}\right)$$

that is, having for all classifiers $h_{\log_g(x_j)}$ that all points $x_i \in X$, $x_i \neq x_j$, are away from its boundary regions in log-space, and that the labels assigned to these points are all the same under noise.

We bound the probability of the negation of this event:

$$\begin{aligned} & \Pr\left(\bigcup_{\substack{i,j \\ i \neq j}} x_i \notin I_{\log_g(x_j)} \cup \bigcup_{i,s'} |e_{i,s'}| \geq \frac{\Delta}{2}\right) \\ & \leq \Pr\left(\bigcup_{\substack{i,j \\ i \neq j}} x_i \notin I_{\log_g(x_j)}\right) + \Pr\left(\bigcup_{i,s'} |e_{i,s'}| \geq \frac{\Delta}{2}\right) \end{aligned}$$

using the union bound.

We start by bounding the first probability, again using the union bound:

$$\begin{aligned} \Pr\left(\bigcup_{\substack{i,j \\ i \neq j}} x_i \notin I_{\log_g(x_j)}\right) & \leq \sum_{\substack{i,j \\ i \neq j}} \Pr(x_i \notin I_{\log_g(x_j)}) \\ & = \sum_{\substack{i,j \\ i \neq j}} \frac{\Delta}{2} \leq \frac{n^{2c}\Delta}{2} \end{aligned}$$

By setting $t \geq 3c$, we have $\Delta \leq 4n^{-t} \leq 4n^{-3c}$, which allows us to bound this first probability by $\delta/4$ when $c \geq \log_n(8/\delta)$.

As for the second probability above, we have

$$\begin{aligned} \Pr\left(\bigcup_{i,s'} |e_{i,s'}| \geq \frac{\Delta}{2}\right) & \leq \sum_{i,s'} \Pr\left(|e_{i,s'}| \geq \frac{\Delta}{2}\right) \\ & \leq \frac{4n^{2c}}{\Delta^2 R} \end{aligned}$$

using the union bound and Eq. (K4). By setting $R \geq \frac{4n^{2(t+c)}}{\delta} \geq \frac{16n^{2c}}{\Delta^2 \delta}$ (since $\Delta \geq 2n^{-t}$), we can bound this second probability by $\delta/4$ as well, which gives:

$$\begin{aligned} & \Pr\left(\operatorname{argmin}_{x \in X} \tilde{\mathcal{L}}(\log_g(x)) = \operatorname{argmin}_{x \in X} \mathcal{L}(\log_g(x))\right) \\ & \geq 1 - \Pr\left(\bigcup_{\substack{i,j \\ i \neq j}} x_i \notin I_{\log_g(x_j)} \cup \bigcup_{i,s'} |e_{i,s'}| \geq \frac{\Delta}{2}\right) \\ & \geq 1 - \delta/2 \end{aligned}$$

□

Lemma 7. *For a training set of size n^c such that $c \geq \log_n\left(\frac{\log(\delta/2)}{\log(1-2\varepsilon)}\right)$, then $s' = \log_g(\operatorname{argmin}_{x \in X} \mathcal{L}(\log_g(x)))$ is within ε distance of the optimal s with probability:*

$$\Pr\left(\frac{|s' - s|}{p-1} \leq \varepsilon\right) \geq 1 - \frac{\delta}{2}$$

Proof. We achieve this result by proving:

$$\Pr \left(\frac{|s' - s|}{p-1} \geq \varepsilon \right) \leq \frac{\delta}{2}$$

This probability is precisely the probability that no $\log_g(x) \in \log_g(X)$ is within ε distance of s , i.e.,

$$\Pr \left(\bigcap_{x \in X} \log(x) \notin [s - \varepsilon(p-1), s + \varepsilon(p-1)] \right)$$

As the elements of the training set are all i.i.d., we have that this probability is equal to

$$\Pr(\log(x) \notin [s - \varepsilon(p-1), s + \varepsilon(p-1)])^{|X|}$$

Since all the datapoints are uniformly sampled from \mathbb{Z}_p^* , the probability that a datapoint is in any region of size $2\varepsilon(p-1)$ is just 2ε . With the additional assumption that $|X| = n^c \geq \log_{1-2\varepsilon}(\delta/2)$ (and assuming $\varepsilon < 1/2$), we get:

$$\Pr \left(\frac{|s' - s|}{p-1} \geq \varepsilon \right) \leq (1 - 2\varepsilon)^{\log_{1-2\varepsilon}(\delta/2)} = \frac{\delta}{2}$$

□

Lemma 6 and Lemma 7 can be used to prove:

Corollary 1. *For a training set of size n^c such that $c \geq \max \left\{ \log_n(8/\delta), \log_n \left(\frac{\log(\delta/2)}{\log(1-2\varepsilon)} \right) \right\}$, a $t \geq 3c$ in the definition of Δ , and a number of circuit evaluations per*

inner product $R \geq \frac{4n^{2(t+c)}}{\delta}$, then our optimization algorithm returns a variational parameter $g^{s'}$ such that

$$\Pr \left(\frac{|s' - s|}{p-1} \leq \varepsilon \right) \geq 1 - \delta$$

From here, we notice that, when we apply Corollary 1 for $\varepsilon' \leq \frac{\Delta}{2}$, our optimization algorithm returns an s' such that, with probability $1 - \delta$, the set $I_{s'}$ is equal to I_s and is of size $(p-1)(1-2\Delta)$. In the event where $|s' - s|/(p-1) \leq \varepsilon' \leq \frac{\Delta}{2}$, we can hence bound the accuracy of the noisy classifier:

$$\begin{aligned} \text{Acc}_{\tilde{h}_{s'}}(f_s) &= \frac{1}{p-1} \sum_{x \in \mathcal{X}} \Pr \left(\tilde{h}_{s'}(x) = f_s(x) \right) \\ &\geq \frac{1}{p-1} \sum_{x \in I_s} \Pr \left(\tilde{h}_{s'}(x) = f_s(x) \right) \\ &\geq (1 - 2\Delta) \min_{x_i \in I_s} \Pr \left(|e_{i,s'}| \leq \frac{\Delta}{2} \right) \\ &\geq (1 - 2\Delta) \left(1 - \frac{4}{\Delta^2 R} \right) \\ &= 1 - \left(2\Delta \left(1 - \frac{4}{\Delta^2 R} \right) + \frac{4}{\Delta^2 R} \right) \end{aligned}$$

with probability $1 - \delta$.

We now set $t \geq \max \{3 \log_n(8/\delta), \log_n(16/\varepsilon)\}$, $\varepsilon' = n^{-t}$ and $R \geq \max \left\{ \frac{4n^{2(t+c)}}{\delta}, \frac{128}{\varepsilon^3} \right\}$, such that $2\varepsilon' = 2n^{-t} \leq \Delta \leq 4n^{-t} \leq \frac{\varepsilon}{4}$, $(1 - \frac{4}{\Delta^2 R}) \leq 1$ and $\frac{4}{\Delta^2 R} \leq \frac{\varepsilon}{2}$. Using these inequalities, we get

$$\text{Acc}_{\tilde{h}_{s'}}(f_s) \geq 1 - \varepsilon$$

with probability $1 - \delta$, which proves Theorem 3.